

Cleveland State University  
**EngagedScholarship@CSU**



---

ETD Archive

---

2015

# Solute Partitioning in Elastin-Like Polypeptides: a Foundation for Drug Delivery Applications

Eric Helm  
*Cleveland State University*

Follow this and additional works at: <https://engagedscholarship.csuohio.edu/etdarchive>

 Part of the [Biomedical Engineering and Bioengineering Commons](#)

**How does access to this work benefit you? Let us know!**

---

## Recommended Citation

Helm, Eric, "Solute Partitioning in Elastin-Like Polypeptides: a Foundation for Drug Delivery Applications" (2015). *ETD Archive*. 471.  
<https://engagedscholarship.csuohio.edu/etdarchive/471>

This Thesis is brought to you for free and open access by EngagedScholarship@CSU. It has been accepted for inclusion in ETD Archive by an authorized administrator of EngagedScholarship@CSU. For more information, please contact [library.es@csuohio.edu](mailto:library.es@csuohio.edu).

**SOLUTE PARTITIONING IN ELASTIN-LIKE POLYPEPTIDES: A  
FOUNDATION FOR DRUG DELIVERY APPLICATIONS**

ERIC HELM

Bachelor of Science in Chemistry

Kent State University

December 2001

Submitted in partial fulfillment of requirements for the degree

**MASTER OF SCIENCE IN CHEMICAL ENGINEERING**

at the

**CLEVELAND STATE UNIVERSITY**

December 2015

We hereby approve this thesis for  
Eric Helm  
Candidate for the Master of Science in Chemical Engineering degree for the  
Department of Chemical and Biomedical Engineering  
and the CLEVELAND STATE UNIVERSITY  
College of Graduate Studies by

---

Thesis Chairperson, Dr. Nolan B. Holland  
Department of Chemical and Biomedical Engineering  
Cleveland State University

---

Date

---

Thesis Committee Member, Dr. Rolf Lustig  
Department of Chemical and Biomedical Engineering  
Cleveland State University

---

Date

---

Thesis Committee Member, Dr. David Anderson  
Department of Chemistry  
Cleveland State University

---

Date

Date of Defense: November 17, 2015

## ACKNOWLEDGEMENTS

First, I would like to thank my academic advisor, Dr. Nolan B. Holland, and my colleagues in his laboratory. During my research, Dr. Holland's guidance and his willingness to answer and ask questions has helped me gain a better understanding of the material. It has been a great experience to work in his laboratory. From the first day I joined the research team my lab mates were friendly, helpful, and encouraging.

I would like to thank my defense committee members Dr. David Anderson and Dr. Rolf Lustig for taking time out of their schedule to review my thesis. Dr. Anderson's knowledge in separation science helped me expand on several analytical techniques and his guidance is appreciated. I am very grateful for the addition of Dr. Lustig to my committee. His advice and encouragement, during my study at CSU, has helped me to stay focused on success.

Also, I would like to thank Dr. Jorge Gatica and Becky Laird for their guidance. They made the enrollment process into the chemical engineering program and my transition into the university a pleasant experience. I am very pleased with the education I received at CSU and especially enjoyed Dr. Gatica's courses.

Finally, I would also like to thank my family, especially my mother. Throughout my life, she has always been supportive and encouraging.

**SOLUTE PARTITIONING IN ELASTIN-LIKE POLYPEPTIDES: A  
FOUNDATION FOR DRUG DELIVERY APPLICATIONS**

**ERIC HELM**

**ABSTRACT**

Elastin-like polypeptides (ELPs) are a class of biopolymers with the potential to function as a novel drug delivery platform. These protein based polymers are composed of the repeating pentapeptide sequence  $(G\alpha G\beta P)_n$  where  $n$  is the number of pentapeptide repeats while  $\alpha$  and  $\beta$  are guest amino acid residues. ELP constructs have been designed to respond to various external stimuli including temperature, pH, and ionic strength where their response to these stimuli results in the separation of the ELP from solution. This phase separation results in a two-phase system consisting of a protein poor supernatant phase and a protein rich coacervate phase.

Under certain conditions select ELP constructs are able to self assemble into micellar structures of nanometer scale when raised above their transition temperature. The micellar architecture consists of an inner hydrophobic core, with a composition like that of the protein rich coacervate phase, surrounded by hydrophilic head groups. For the use of ELP micelles as a drug delivery platform these particles should possess the ability to encapsulate solute molecules. In this study, solute solubility within the micelle core was investigated by measuring the partition coefficients of several solutes in five different ELP two-phase systems, then all data was fit to a linear free energy relationship (LFER) model to provide insight into the dominate interactions governing solute

partitioning in ELP systems. From the LFER it is shown that the cavity formation energy, solute size, and the solvents hydrogen bond acidity are important parameters governing solute partitioning in the ELP solvents investigated. Additionally, the partition coefficients provide a measurement of ELP phase hydrophobicity from which the development of future ELP constructs is possible.

# TABLE OF CONTENTS

	<b>Page</b>
<b>ABSTRACT</b>	iv
<b>LIST OF TABLES</b>	viii
<b>LIST OF FIGURES</b>	x
<b>CHAPTER</b>	
<b>I. INTRODUCTION</b>	1
1.1 Elastin-like Polypeptides	1
1.2 Solute Partitioning	14
1.3 Liquid Chromatography	22
<b>II. OBJECTIVE</b>	41
<b>III. MATERIALS AND METHODS</b>	44
3.1 Protein Synthesis and Purification	44
3.2 Solutes Investigated	46
3.3 Master Stock Solute Solution Preparation	47
3.4 Partition Coefficient Calculation Procedure	48
3.5 Partitioning	48
3.6 High Performance Liquid Chromatography Setup	50
<b>IV. RESULTS AND DISCUSSION</b>	53
<b>V. CONCLUSION</b>	75

<b>BIBLIOGRAPHY</b>	77
<b>APPENDIX</b>	91
Appendix A	91
Lysogeny Broth (LB) Media Preparation	91
Protein Expression	91
Appendix B	95
Protein Extraction Protocol	95
Protein Purification by Inverse Temperature Cycling	95
Appendix C	101



## LIST OF TABLES

<b>Table</b>		<b>Page</b>
Table 1.1	Selected $T_i$ Values Obtained from Urry's Hydrophobicity Scale	7
Table 1.2	$T_i$ Values for Histidine and Glutamic Acid Obtained from Urry's Hydrophobicity Scale.	10
Table 1.3	Solute and Solvent Descriptors for LFER	18
Table 1.4	Selected McGowan Characteristic Atomic Volumes	20
Table 1.5	Common Types of Modified Silica HPLC Stationary Phases	36
Table 3.1	Amino Acid Sequences for all Proteins Investigated	46
Table 4.1	Results from HPLC DAD Detector Linearity Check	54
Table 4.2	Measured Coacervate Masses for $(V_3(VH)_3)_4$ Protein System	56
Table 4.3	Comparison of Partition Coefficients using the Coacervate Mass and Protein Peak Area Methods of Calculation	60
Table 4.4	Final Partition Coefficients Results Table	61
Table 4.5	Literature Values of Solute Descriptors	62
Table 4.6	Calculated Solvent Descriptors using all Interaction Parameters	63
Table 4.7	Objective Function Values when Interaction Descriptor was Eliminated from LFER	64

Table 4.8	Calculated Solvent Descriptors using Selected Interaction Parameters	66
Table 4.9	Solute Descriptors for Doxorubicin	71
Table 4.10	Solvent Descriptors Obtained from Linear Regression of Solute Set with and without Including Doxorubicin	72
Table 4.11	Calculated Solute Partition Coefficients	74

## LIST OF FIGURES

<b>Figure</b>		<b>Page</b>
Figure 1.1	ELP solution phase separation behavior.	3
Figure 1.2	Transition temperature as a function of pH for glutamic acid and histidine containing ELPs.	10
Figure 1.3	Molecular structure of phenol.	20
Figure 1.4	Chromatographic process showing the separation of a two component mixture as it travels through a chromatography column.	24
Figure 1.5	Typical liquid chromatogram.	26
Figure 1.6	Hypothetical Van Deemter plot for various stationary phase particle sizes.	29
Figure 1.7	Schematic diagram of an HPLC system.	31
Figure 1.8	Schematic diagram of Ryeodyne injection valve.	33
Figure 1.9	Hypothetical silica stationary phase bead.	35
Figure 1.10	Schematic diagram showing DAD detector optics.	38
Figure 1.11	Chromatogram obtained from an HPLC DAD detector.	39
Figure 2.1	Three armed star ELP.	41

Figure 2.2	Micelle structure of Foldon-ELP.	42
Figure 3.1	Structures for all compounds investigated in this study.	47
Figure 3.2	Representative chromatograms for solvent/protein systems.	52
Figure 4.1	Plot of original data and averaged coacervate mass data for ethyl paraben in the $(V_3(VH)_3)_4$ protein system.	56
Figure 4.2	Plot of coacervate mass fraction as a function of $(GVGVP)_{40}$ protein peak area.	58
Figure 4.3	Example results using coacervate mass and protein peak area calculation.	60
Figure 4.4	$\text{Log}(K)_{\text{fit}}$ vs. $\text{log}(K)_{\text{exp}}$ using all interaction parameters.	63
Figure 4.5	$\text{Log}(K)_{\text{fit}}$ vs. $\text{log}(K)_{\text{exp}}$ for selected interaction parameters.	65
Figure 4.6	Chromatogram of investigated ELP constructs.	69
Figure 4.7	Molecular structure of doxorubicin.	70
Figure 4.8	Partitioning data for doxorubicin.	72
Figure 4.9	$\text{Log}(K)_{\text{fit}}$ vs. $\text{log}(K)_{\text{exp}}$ with doxorubicin included in the solute set.	73

# CHAPTER I

## INTRODUCTION

### 1.1 Elastin-like Polypeptides

Elastin-like polypeptides (ELP) are a class of biopolymers whose amino acid composition and sequence mimics that of mammalian elastin. Elastin is found throughout the animal kingdom typically making up the predominant fraction of extracellular matrix in tissues such as arterial blood vessels, lung parenchyma, elastic ligaments, ear cartilage, and skin. [1] Its function in these tissues is to provide an elastic characteristic, giving them the ability to expand and contract without mechanical failure. In fact, during the average human life span the heart will beat more than 2.5 billion times. During this process the aorta elastin transitions through billions of cycles of extension and recoil without mechanical failure, showing the remarkable properties of elastin as a biomaterial. [1] Naturally occurring elastin contains a repeat of the pentapeptide sequence GVGVP. To expand upon this composition, the ELP class of biopolymers is built from the generic pentapeptide sequence  $(G\alpha G\beta P)_n$ , where  $n$  is the number of pentapeptide repeats, and  $\alpha$  and  $\beta$  are amino acid guest residues. Substitution of different

amino acids into the  $\alpha$  and  $\beta$  positions as well as altering the number of pentapeptide repeats provides a large library of ELP compositions for study. It has been discovered, in order to maintain phase transition behavior and elastic characteristics of the ELP construct, the guest residue  $\alpha$  can be replaced with any amino acid except for proline while  $\beta$  can be replaced with any amino acid. [2]

Current production of elastin-like polypeptides is performed using an *Escherichia Coli* (*E. coli*) bacterial host. Several types of plasmid construction techniques capable of ELP production have been presented in the literature. [3, 4, 5] One plasmid construction technique commonly used to build the appropriate plasmid is called recursive directional ligation (RDL). [3, 6] This technique begins with the design of an *E. coli* expression vector compatible with the ELP gene. Once the appropriate cut sites are in place short oligonucleotide segments encoding the amino acid sequence ( $G\alpha G\beta P$ ) are inserted. This process is repeated until the desired ELP sequence has been inserted into the vector, then the final vector is transformed into an *E. coli* host for protein expression. Using genetic engineering allows the production of research quantities of ELP and precise control over ELP chain length and amino acid sequence, characteristics that give ELPs their functionality.

### 1.1.1 ELP transition temperature

One interesting feature of elastin-like polypeptides is their display of lower critical solution temperature (LCST) behavior. When the temperature of an aqueous solution of ELP is raised above its transition temperature, hydrophobic domains within

the protein backbone associate causing the protein to aggregate, resulting in a cloudy solution. The temperature at which the solution begins to cloud is known as the solution transition temperature ( $T_t$ ). When solutions are allowed to sit above their transition temperature settling of the protein layer occurs resulting in a two-phase system composed of a protein rich lower “coacervate” phase made of 40-50% protein by mass and a protein poor upper “supernatant” phase (Figure 1.1). [2]

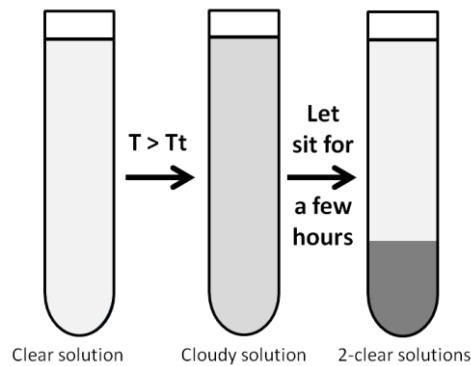


**Figure 1.1** ELP solution phase separation behavior modified from reference [2].

This phase transition is completely reversible. Upon cooling the solution below its transition temperature, the protein dissolves back into solution. The transition temperature is dependent on both solution and ELP molecular characteristics. Characteristics, such as ionic concentration, pH, ELP concentration, ELP chain length, and amino acid composition, can be adjusted in order to alter the solution transition temperature.

### *Inorganic salt influence on ELP transition temperature*

Inorganic salt concentration has been known to have a strong effect on protein solubility. Research has shown that ionic salts, more often the salt anion, can influence the transition temperature of ELPs. [7] For the kosmotrophic anions;  $F^-$ ,  $H_2PO_4^-$ ,  $S_2O_3^{2-}$ ,  $SO_4^{2-}$ ,  $CO_3^{2-}$ , and  $Cl^-$  a linear relationship exists between transition temperature and ion concentration where  $T_0$  is the solution transition temperature without the addition of salt,  $[M]$  is the salt concentration in molar units, and  $c$  is a constant with units of temperature/molarity, Eq. (1.1).

$$T_t = T_0 + c[M] \quad (1.1)$$

For these anions, their addition to an ELP solution results in a decrease in the transition temperature due to polarization of water molecules and a reduction in hydrogen-bonding strength between water molecules and hydrophilic regions of the ELP. Other anions have been shown to increase the transition temperature. [7, 8] In contrast with the kosmotrophic anions these anions;  $SCN^-$ ,  $I^-$ ,  $ClO_4^-$ ,  $Br^-$ , and  $NO_3^-$  show a nonlinear response in ELP transition temperature as a function of anion concentration. This response has been characterized by adding a binding isotherm to Eq. (1.1), Eq. (1.2),

$$T_t = T_0 + c[M] + \frac{B_{max}K_A[M]}{1+K_A[M]} \quad (1.2)$$

where  $K_A$  is the apparent equilibrium constant and  $B_{max}$  (units of temperature) is a constant interpreted as the increase in ELP transition temperature in a saturated anion solution.



### *Influence of protein concentration and chain length on ELP transition temperature*

ELP concentration and chain length have a significant influence on the transition temperature. Research performed by Meyer and Chilkoti has shown a linear relationship between transition temperature and the logarithm of the protein concentration for dilute ELP solutions, where  $C_c$  is the critical concentration in molar units,  $T_{t,c}$  is the critical

$$T_t = T_{t,c} + k_c \ln\left(\frac{C_c}{C}\right) \quad (1.3)$$

$$k_c = \frac{k}{L} \quad (1.4)$$

transition temperature,  $k_c$  is a constant in units of °C, and  $L$  is the number of pentapeptide repeats, Eq. (1.3). [9] In this model the critical values of concentration and temperature are the concentration and temperature at which the transition temperature reaches a minimum and is no longer dependent on ELP chain length. This model has been further advanced by Ghoorchian and Holland during their investigation into a three-armed star ELP (trimer). [10] Fitting their data, for the trimer construct, to Eq. (1.3) resulted in a slightly lower critical transition temperature than expected and the critical concentration was one order of magnitude higher than expected. Due to these discrepancies the concentration units were changed to polymer coil volume and the critical concentration was arbitrarily defined as 1. Once again the data was fit to Eq. (1.3), but in this case a better fit was achieved for the trimer construct resulting in a single  $T_{t,c}$  independent of polymer chain length.

### *Influence of amino acid composition on ELP transition temperature*

To explore the influence of ELP amino acid composition on transition temperature, Urry has developed a hydrophobicity scale by varying the ELP amino acid composition under common solution conditions (pH 7.5, 0.15 M NaCl, 0.01 M phosphate, protein concentration: 40 mg/mL). [2] Urry synthesized several high molecular weight ELP constructs based on the model poly[ $f_v$ (GVGVVP), $f_x$ (GXGVVP)], where  $f_v$  and  $f_x$  were mole fractions spanning a range between 0 and 0.5 and the guest residue, X, was one of the 20 naturally occurring amino acids. The data showed a linear relationship between mole fraction,  $f_x$ , and solution transition temperature for every ELP composition investigated. Extrapolation to a common value of  $f_x = 1$  was performed to determine the influence of that specific amino acid residue on the hydrophobicity of the complete ELP construct. Hydrophobicity was measured by the transition temperature where more hydrophobic amino acid residues resulted in a lower  $T_t$ . Using this hydrophobicity scale the transition temperature of an experimental ELP can be estimated by adding the influence from each guest residue. For example, according to Urry's hydrophobicity scale (Table 1.1) the ELP construct [(GVGVVP)<sub>38</sub>(GFGVP)<sub>2</sub>] results in a transition temperature of 21°C.

$$T_t = \frac{(38)(24^\circ\text{C}) + (2)(-30^\circ\text{C})}{(38 + 2)} = 21^\circ\text{C}$$

**Table 1.1** Selected Values Obtained from Urry's Hydrophobicity Scale [2]

Residue	Letter	T <sub>t</sub> (°C)
Phenylalanine	F	-30
Valine	V	24

*Influence of added hydrophobicity on ELP transition temperature*

Changing the amino acid composition of an ELP construct is not the only method of altering the transition temperature by changing ELP hydrophobicity. Chilkoti et al. has demonstrated that covalently bonding a hydrophobic drug molecule to an ELP can alter the solution T<sub>t</sub>. [11] In this study, doxorubicin was covalently attached to an ELP through an acid-labile linker. After the synthesis and purification of the ELP-dox conjugate, the Chilkoti group noticed the transition temperature of the conjugate was 10°C lower than that of the pure ELP. This example shows how changing the hydrophobicity of the ELP construct by attachment of a drug molecule can change the transition temperature, similar to the behavior observed when changing the amino acid composition of the ELP. By attaching a hydrophobic drug to the ELP, the overall molecule has become more hydrophobic resulting in a decrease in the transition temperature.

*Influence of solution pH on ELP transition temperature*

When amino acids capable of accepting or donating a proton are incorporated into the ELP structure the transition temperature becomes a function of the solutions pH. Chilkoti et al. has investigated this behavior by varying the solution pH for two pH

responsive ELP constructs, one containing acidic glutamic acid residues and the other containing basic histidine residues, then measuring the solutions  $T_t$ . [12] Initially Chilkoti's group determined that for all solution pH values investigated a linear relationship was observed between the transition temperature and log protein concentration, Eq. (1.3). Then, using the Henderson-Hasselbach equation Chilkoti's group developed a relationship between transition temperature, solution pH, and ELP pKa, Eq. (1.5).

$$T_t = T_{\text{pro}} + \frac{T_{\text{depro}} - T_{\text{pro}}}{1 + 10^{(\text{pKa} - \text{pH})}} \quad (1.5)$$

Equation (1.5) describes the behavior of ELPs containing both acidic and basic amino acid residues, where  $T_{\text{depro}}$  and  $T_{\text{pro}}$  are the transition temperatures of the fully deprotonated and protonated ELP respectively. For acidic ELP residues  $T_{\text{depro}}$  is greater than  $T_{\text{pro}}$  therefore, according to Eq. (1.5), the solution transition temperature would increase with pH. For basic ELP residues  $T_{\text{pro}}$  is greater than  $T_{\text{depro}}$  resulting in a decrease in transition temperature with increasing solution pH. Identical results were observed by our group for glutamic acid and histidine containing ELPs. Transition temperatures were measured as a function of solution pH for a glutamic acid containing ELP,  $(\text{VEV})_{12}$ , [13] and histidine containing ELP,  $(\text{V}_3(\text{VH})_3)_4$  [14] then, Eq. (1.5) was used to model the data (Figure 1.2).

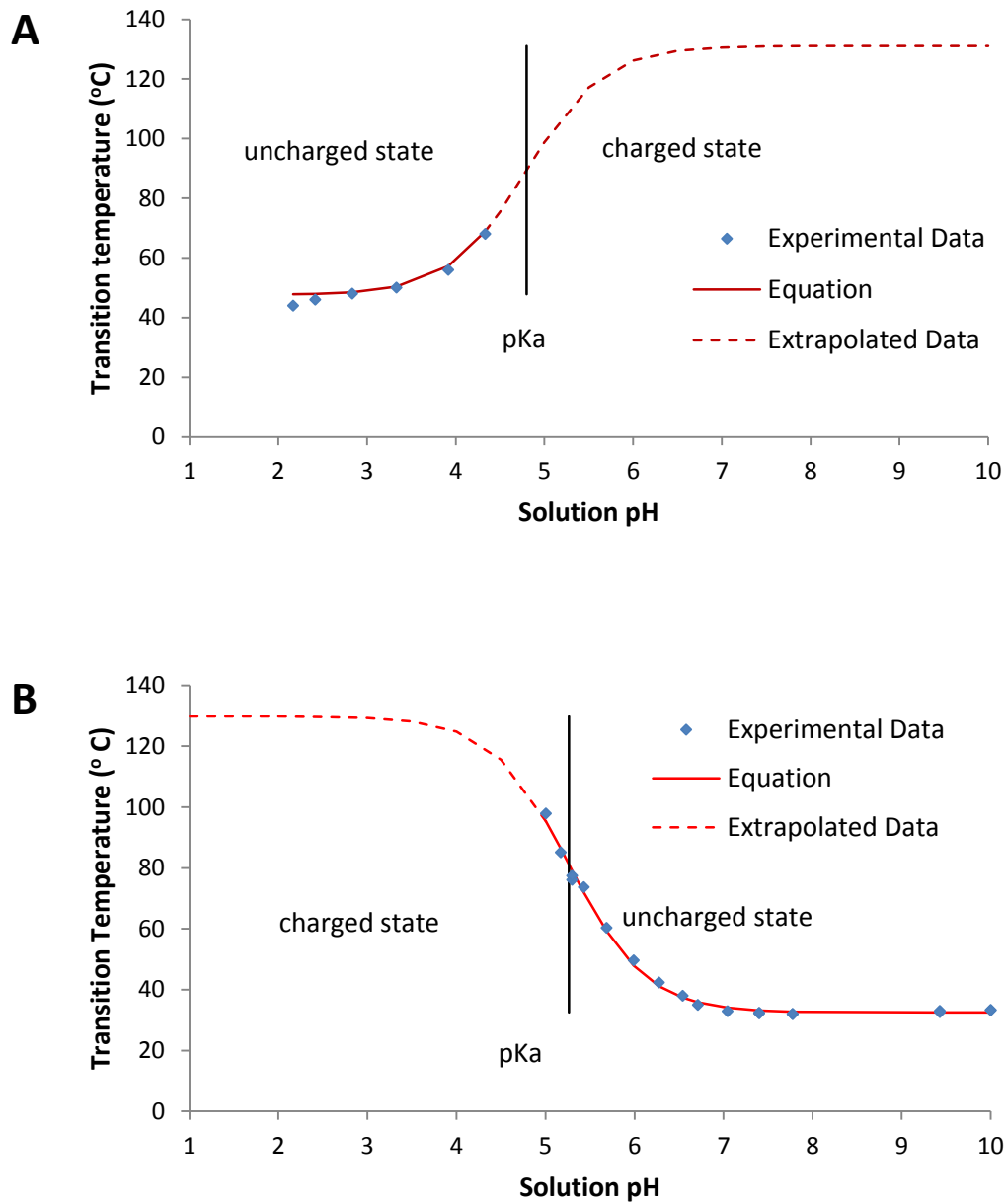


**Figure 1.2** Transition temperature as a function of solution pH for A) glutamic acid containing ELP construct (VEV)<sub>12</sub> at a protein concentration of 10  $\mu$ M in PBS (150 mM NaCl, 0.01 M phosphate) with a pKa of 4.8 and B) histidine containing ELP construct (V<sub>3</sub>(VH)<sub>3</sub>)<sub>4</sub> at a protein concentration of 100  $\mu$ M in PBS with a pKa of 5.3. Experimental data was modeled using Eq. (1.5).

The results obtained from our group also follow the trends observed in Urry's hydrophobicity scale. According to Urry's scale, ELP constructs become more hydrophilic in their charged state, indicated by a higher  $T_t$  (Table 1.2). As shown in Figure 1.2, for acidic as well as basic amino acid containing ELPs, the  $T_t$  of the ELP construct in its charged state is greater than the  $T_t$  in its uncharged state.

**Table 1.2**  $T_t$  Values for Histidine and Glutamic Acid Obtained from Urry's Hydrophobicity Scale [2]

Residue	Abbreviation	Letter	$T_t$ (°C)
Histidine	His	H	-10
Histidine	His <sup>+</sup>	H <sup>+</sup>	30
Glutamic acid	Glu	E	30
Glutamate	Glu <sup>-</sup>	E <sup>-</sup>	250

### 1.1.2 Elastin-like polypeptides for use in drug delivery

The use of elastin-like polypeptides for biological applications has been studied for many years. Research has shown these materials are biocompatible, biodegradable, and non-immunogenic. [15] Since the transition temperature of these materials can be finely controlled the main focus of this research has been directed toward investigation into applications involving drug delivery. Potential ELP drug delivery systems are constructed by either: directly attaching the drug molecule to the carrier or by encapsulation of the drug molecule within a hydrophobic environment.

### *Drug delivery by ELP-drug conjugation*

Chilkoti et al. has demonstrated the direct attachment method of drug delivery by covalently bonding the chemotherapeutic drug, doxorubicin, to an ELP for use in cancer treatment. [11] The drug was bound to the ELP through an acid-labile hydrazone linker, enabling release of the drug within low pH environments. The authors state two reasons for using an ELP as the drug carrier. First, when drugs are bound to large macromolecules, such as an ELP, tumor permeability and retention within tumor cells increases compared to the free drug, an effect known as the enhanced permeability and retention effect (EPR). [16] Second, if the tumor site is heated above the transition temperature of the ELP-doxorubicin conjugate (ELP-dox), accumulation of the drug within the tumor can occur resulting in a more efficient drug delivery system. It is interesting to note the Chilkoti group has previously shown that fluorescent tagged-ELP conjugates will accumulate within tumors that have been heated above the ELP transition temperature and this accumulation only occurs when the local temperature is above the ELP transition temperature. [17, 18]

The final results of this study showed a near-equivalent cytotoxicity of the ELP-dox conjugate and free doxorubicin. After comparing the cellular distribution of the ELP-dox conjugate to free doxorubicin it was shown that the ELP-dox was concentrated in the cell cytoplasm, while the free doxorubicin accumulated within the cell nucleus. Given this difference in accumulation site, yet an equivalent cytotoxicity of the ELP-dox and free doxorubicin, the results suggest a different mechanism of cytotoxicity for the

ELP bound drug compared to the free drug. Similar results were obtained by Moktan et al. when investigating a paclitaxel-ELP conjugate where the authors, once again, explain this behavior based on a different mechanism of cytotoxicity between the ELP bound and free drug. [19]

#### *Drug delivery by ELP-drug encapsulation*

A study conducted by Wright et al. involved the synthesis and characterization of several block ELPs one of which was capable of self assembly into micelles of nanometer size. [20] In dilute concentrations this block polymer formed spherical nanoparticles, at 25°C under basic conditions (0.1 M NaOH) or PBS (pH 7.4, 0.15 M NaCl, 0.01 M phosphate), with an average hydrodynamic diameter of 50-90 nm. The authors investigated the potential of these nanoparticles to encapsulate small molecules using two fluorescent dyes, 1-anilinonaphthalene-8-sulfonic acid (1,8-ANS) and Nile Red. Data from this study showed strong association of the dyes with the hydrophobic blocks of the ELP indicating encapsulation of the dye within the micelle core. The authors conclude the dyes did not associate with the hydrophilic blocks of the ELP, which supports the hypothesis that the hydrophobic blocks were exclusively responsible for the encapsulation.

Similar results were observed by Kim et al. during their investigation into disulfide crosslinked, block, ELP micelles loaded with the anti-inflammatory drug dipyridamole (DIP). [21] In this study, 50 nm micelles were loaded with DIP and drug release profiles were measured. The data from the drug release experiments showed an



initial burst release over a 3 hour period followed by an extended release over 40 hours. When the authors changed the length of the ELP hydrophobic block the resulting micelles were of the same diameter, but these micelles were found to release the drug more slowly than did the micelles with the shorter block. The authors suggest this difference in release rate be attributed to the more densely packed micelle core formed by longer hydrophobic blocks, increasing the interactions between the drug molecule and the hydrophobic core.

Drug loaded micelles or nanoparticles are not the only type of drug delivery system designed from ELPs. The objective of a study conducted by Adams et al. was to develop an injectable drug containing ELP depot, from which an antibiotic drug could be slowly released over time. [22] In this study an ELP containing a large percentage of lysine residues was crosslinked to form an injectable gel. After crosslinking, the gel was loaded with two antibiotics and drug release studies were performed. For both antibiotics, cafazolin and vancomycin, the data from the release study showed sustained release over 25 and 520 hours respectively.

While some examples in literature include the loading of elastin-like polypeptides with drug molecules other studies were conducted to show their potential use as an effective drug delivery platform. Certain types of ELPs have been shown to self assemble into micelles of nanoscale size when heated above their transition temperature. Ghoorchian et al. constructed and characterized a three armed star ELP that possesses the ability to form micelles under high pH and low NaCl concentration. [6] This ELP, named H40-foldon, is composed of 40 GVGVP pentapeptide blocks attached to a foldon domain headgroup. When an aqueous solution of H40-foldon is heated above its

transition temperature, spherical micelles of approximately 30 nm in diameter are produced. The micellar architecture consists of an interior composed of the hydrophobic ELP and an exterior decorated by the foldon headgroups. [23] The authors of this study did not drug load these particles, but do suggest their use as a potential drug delivery vehicle.

## 1.2 Solute Partitioning

When a solute is distributed at constant temperature and pressure between multiple solvent phases equilibrium is established when the chemical potential of each species is identical in all phases. [24] The chemical potential of a solute species,  $\mu$ , in a two phase system,  $\alpha$  and  $\beta$ , can be represented by:

$$\mu_{\alpha} = \mu_{\alpha}^{\circ} + (RT)\ln(f_{\alpha}) \quad (1.6)$$

$$\mu_{\beta} = \mu_{\beta}^{\circ} + (RT)\ln(f_{\beta}) \quad (1.7)$$

where  $\mu^{\circ}$  is the standard state chemical potential and  $f$  is the solute activity. The solute activity may be expressed as:

$$f = (\gamma)(X) \quad (1.8)$$

where  $\gamma$  is the phase specific solute activity coefficient and  $X$  is the phase specific solute concentration. At equilibrium; Eq. (1.6), Eq. (1.7), and Eq. (1.8) may be combined and written as Eq. (1.9).

$$\mu_{\alpha}^{\circ} - \mu_{\beta}^{\circ} = (RT)\ln\left(\frac{(\gamma_{\beta})(X_{\beta})}{(\gamma_{\alpha})(X_{\alpha})}\right) \quad (1.9)$$

As a solute concentration approaches infinite dilution, the solute/solvent system behaves more ideally and the activity coefficient approaches 1. Assuming an ideal solution, the Gibbs free energy of transfer for a solute molecule from solvent phase  $\alpha$  to phase  $\beta$  takes the form:

$$\frac{\Delta G_{\text{tr}(\alpha \rightarrow \beta)}}{RT} = \ln\left(\frac{X_{\beta}}{X_{\alpha}}\right) = \ln(K) \quad (1.10)$$

where  $K$  is the partition coefficient of the solute defined as the ratio of solute concentrations between both solvent phases at equilibrium.

### 1.2.1 Methods to determine the partition coefficient

The partition coefficient,  $K$ , is defined as the ratio of solute concentrations between two phases at equilibrium, Eq. (1.11). Zaslavsky describes two methods

$$K_{\beta/\alpha} = \frac{[\text{Solute}]_{\beta}}{[\text{Solute}]_{\alpha}} \quad (1.11)$$

for the determination of the solute partition coefficient. [25] Both methods begin with the addition of the solute to be partitioned to a two-phase solvent system at the desired temperature. After mixing to aid in dissolution of the solute and transfer between the two phases, the solvent system is allowed to phase separate for 12-24 hours or alternatively centrifuged for a shorter period of time.

In the first method, described by Zaslavsky, the above procedure is performed several times using a fixed amount of solute introduced into the system. After phase separation the solvent phases are analyzed and the solute partition coefficient is

determined. In the second method, the partitioning procedure is performed by varying the amount of solute added to the solvent system. Usually, four or five different amounts of solute are added to separately prepared solvent systems of the same composition. After phase separation the solvent phases are analyzed and the partition coefficient of the solute is determined by standard linear regression analysis, defined as the slope of the linear regression line:

$$[\text{Solute}]_{\beta} = K[\text{Solute}]_{\alpha} + b \quad (1.12)$$

where  $[\text{Solute}]$  is the concentration of solute within the respective solvent phase,  $\alpha$  and  $\beta$ . Using this method to calculate  $K$  determines if additional interactions are present that influence the partition process. These additional interactions cause a deviation from the linear behavior described by Eq. (1.12). Zaslavsky showed this deviation from linear behavior while studying the partitioning of egg white lysozyme in an aqueous two-phase solvent system. [25] When lysozyme was partitioned in an aqueous Dex-Ficoll two-phase system containing 0.11 mole/Kg sodium phosphate buffer at pH 7.40, significant deviation from linearity was observed. Partitioning of lysozyme was also performed in the same solvent system containing 0.01 mole/Kg universal buffer at pH 4.4, where linear behavior was observed. These results were explained by the dimerization of lysozyme at alkaline pH, resulting in the observed deviation from Eq. (1.12) due to additional interactions affecting the partitioning behavior. [26]

## 1.2.2 Solute partitioning models

Using solute partition coefficients, many models have been developed to describe the behavior of membrane transfer [27, 28], to determine relative hydrophobicity of organic compounds [29], to model chromatographic retention time [30, 31], to describe surface adsorption [32], and to predict solute solubility [33, 34, 35]. Abraham et al. has developed a solute partitioning model called a linear free energy relationship (LFER), Eq. (1.13), by describing the logarithm of the solute partition coefficient as a linear combination of several interaction parameters, where  $\log SP$  is the logarithm of a solute property typically the solute partition coefficient;  $E$ ,  $S$ ,  $A$ ,  $B$ , and  $V$  are solute descriptors; and  $e$ ,  $s$ ,  $a$ ,  $b$ , and  $v$  are solvent descriptors (Table 1.3). [35, 36, 37, 38, 33]

$$\log SP = eE + sS + aA + bB + vV + c \quad (1.13)$$

**Table 1.3** Solute and Solvent Descriptors for Abraham's Linear Free Energy Relationship

Solute Descriptor	Description
E	The excess molar refractivity parameter in units of $(\text{cm}^3 \text{mol}^{-1})/10$ .
S	The solute dipolarity/polarizability descriptor.
A	The solutes overall hydrogen bond acidity descriptor.
B	The solutes overall hydrogen bond basicity descriptor.
V	The McGowan characteristic volume in units of $(\text{cm}^3 \text{mol}^{-1})/100$ .

Solvent Descriptor	Description
e	Describes the solvents ability to interact with a solute through $\pi$ - and n-electron pairs.
s	Related to the difference in solvent dipolarity/polarizability between the phases.
a	Related to the difference in solvent hydrogen bond acceptor basicity between the phases.
b	Related to the difference in solvent hydrogen bond doner acidity between the phases.
v	Describes the solvents ability to interact with a solute by dispersive forces and/or the energy required to create a cavity in the solvent phase.

In the LFER, the solute descriptor E is the excess molar refractivity and refers to interactions through  $\pi$ - and n- electron pairs. [31] This descriptor is calculated as the difference between, the molar refraction of the solute calculated using McGowan's characteristic volume ( $MR_x$ ), and the molar refraction of an alkane with the same McGowan volume ( $MR_x$ )<sub>alkane</sub>, Eq. (1.14). To calculate  $MR_x$ , Eq. (1.15), uses the McGowan characteristic volume ( $V_m$ ) and, for liquids, the solute index of refraction or, for solids, the hypothetical index of refraction ( $\eta$ ). [39]

$$E = MR_x - (MR_x)_{\text{alkane}} \quad (1.14)$$

$$MR_x = 10 \left( \frac{\eta^2 - 1}{\eta^2 + 2} \right) \left( \frac{V_m}{100} \right) \quad (1.15)$$

$$(MR_x)_{\text{alkane}} = (2.83195) \left( \frac{V_m}{100} \right) + 0.52553 \quad (1.16)$$

The solute descriptor V is the McGowan characteristic volume. This descriptor is a representation of the energy required to separate solvent molecules and create a cavity of suitable size to accommodate the solute. [40] Numerical values of this descriptor are often much larger than the values for the other descriptors in the LFER equation. Therefore, in the LFER equation this descriptor is scaled and used as  $V/100$ . To calculate the McGowan characteristic volume all that is needed is the compound's molecular structure and the list of characteristic atomic volumes determined by Abraham and McGowan. [40] From the compound's molecular structure, the number of each specific atom and the total number of bonds can be determined. The McGowan volume is calculated by summing, for all atom types, the product of the number of atoms multiplied by its characteristic atomic volume then subtracting the total number of bonds multiplied

by  $6.56 \text{ cm}^3 \text{ mol}^{-1}$ , Eq. (1.17). It should be noted that in the calculation of the McGowan volume, the number of bonds are multiplied by  $6.56 \text{ cm}^3 \text{ mol}^{-1}$  no matter whether they are single, double, or triple bonds.

$$V = \sum(\text{\#of atoms})(\text{characteristic atomic volume}) - (\text{\# of bonds})(6.56) \quad (1.17)$$

**Table 1.4** Selected McGowan Characteristic Atomic Volumes [40]

Element	Characteristic Atomic Volume ( $\text{cm}^3 \text{ mol}^{-1}$ )
Carbon	16.35
Hydrogen	8.71
Oxygen	12.43

For each bond between atoms,  $6.56 \text{ cm}^3 \text{ mol}^{-1}$  is to be subtracted

For example, phenol is a simple aromatic compound with the molecular formula  $\text{C}_6\text{H}_6\text{O}$  (Figure 1.3) and contains a total of 13 bonds. Thus, for phenol  $V$  is calculated as  $77.5 \text{ cm}^3 \text{ mol}^{-1}$ .

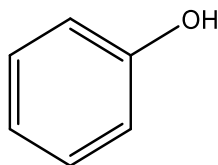


**Figure 1.3** Molecular structure of phenol

$$V = (6)(16.35) + (6)(8.71) + 12.43 - (13)(6.56) = 77.5$$

The S descriptor is a measure of the solutes ability to interact in dipole-dipole and dipole-induced dipole interactions while the A and B descriptors represent the interactions of hydrogen bond acidity and hydrogen bond basicity respectively. These three descriptors can be obtained from gas liquid chromatography measurements, water-solvent partitioning, and molecular modeling. [41, 42, 43] Currently, with the vast number of Abraham solvent and solute descriptors available, the solute descriptors (S, A, and B) can be obtained through multiple linear regression using Eq. (1.13). This method is commonly employed to determine solute descriptors when solubility data for the solute is known. For example, Bradley et al. calculated the S, A, and B Abraham solute descriptors for trans-cinnamic acid (CA) from published solubility data of (CA) in 26 solvents all of which have Abraham solvent parameters (e, s, a, b, c). [44] This group began by calculating the E and V descriptors from chemical structure by comparison with other structurally similar compounds, such as ethyl benzoate, benzoic acid, and ethyl cinnamate. Next, a total of 45 LFER equations were constructed by combining the solubility data with (CA) partition coefficients measured in several different solvent systems. Finally, these LFER equations were solved by regression to determine the values of S, A, and B that gave the best fit of experimental and calculated properties. The final results from this group showed that unknown Abraham solute descriptors can be calculated from measured solute solubility in several solvents provided that the Abraham solvent descriptors for these solvents are available. An identical procedure as that above has been applied by other authors with similar results. [45, 46]



## 1.3 Liquid Chromatography

In the early 1900's Russian botanist, Mikhail S. Tswett focused his study on the separation of leaf pigments obtained from plant material by solvent extraction. [47] His experiments centered on using a glass tube or column packed with fine particles of calcium carbonate to perform the separation of the pigments. [48] The experiment was performed by using slight pressure or suction to flow a solvent through the packed column until the particle bed was equilibrated. Next the plant extract was applied to the column inlet, once the extract passed into the particle bed additional solvent was used to move the material through the column. What resulted was the separation of the leaf pigments into different colored bands as they passed through the column packing. What was born was a new separation technique based upon the different interactions of a solute with a liquid and solid phase. This technique was called liquid chromatography.

### 1.3.1 Advantages of Liquid Chromatography

Analytical liquid chromatography is a technique used in analytical chemistry to separate a matrix into its individual components for quantitative and/or qualitative analysis. With analytical techniques such as UV-VIS spectroscopy, the total absorption signal is the sum of the absorptions for all species present including the matrix background. For the quantification of an analyte by UV-VIS spectroscopy, previous knowledge of sample composition is required. Using this knowledge all background interferences can be subtracted from the total absorption signal, leaving the contribution to the signal from the analyte of interest. This remaining absorption signal can then be used

for quantification of the analyte. While this procedure works well for a simple matrix of one or two components, more complex matrices require an additional dimension to the analysis. This additional dimension is usually in the form of a separation of the matrix analytes before analysis. Using liquid chromatography to perform this separation has the advantage of separating the matrix into individual components for evaluation separately. This usually results in an increase in sensitivity and a lower limit of detection. Additionally, with the use of chromatography routine evaluation of more complex samples, such as biological fluids, is possible.

### 1.3.2 Industrial uses of Liquid Chromatography

Since Tsweet's experimentation on the separation of plant pigments, liquid chromatography has proven to be a versatile and robust method for the quantification of simple and complex sample matrices. This versatility is displayed by the large range of industries that have adopted this technique as a standard method of analysis. The pharmaceutical and chemical processing industries commonly use liquid chromatography during the synthesis of pharmaceutical drugs and other chemical commodities. [49] Liquid chromatography provides these industries with the ability to determine when a chemical reaction is complete and what reaction impurities were produced. With this information companies can determine when problems arise and how to correct them before a dangerously contaminated product enters the consumer market.

### 1.3.3 Chromatography Theory

The separation of analytes by liquid chromatography relies on the difference in analyte interaction between the stationary and mobile phases. A typical chromatographic process is depicted in Figure 1.4 [50].

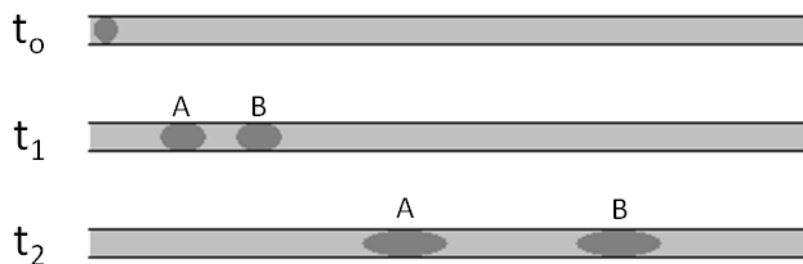


**Figure 1.4** Chromatographic process showing the separation of a two component mixture as it travels through a chromatography column. Figure modified from reference [50].

In Figure 1.4 at time  $t_0$ , a two component mixture is introduced onto a liquid chromatography column then, a continuous supply of mobile phase is introduced to transport the analyte material through the column. As the compounds move through the chromatographic column they partition between the stationary and mobile phases determined by their relative affinity for each phase. If a compound has a stronger interaction with the stationary phase, then that compound will spend a greater proportion of its time on the column adsorbed to the stationary phase. Since the velocity of the stationary phase is zero these compounds move through the column slowly. The opposite is true for compounds with a stronger mobile phase interaction. These compounds spend

a greater proportion of their time on the column within the mobile phase. Compounds within the mobile phase move at the mobile phase velocity resulting in rapid migration through the column. In Figure 1.4, the differences in relative interaction begin to show at time  $t_1$  by separation of the sample matrix into its individual components A and B. Shown in Figure 1.4, compound A has a greater relative affinity for the stationary phase while compound B has a greater relative affinity for the mobile phase.

### *Column Efficiency and Band Broadening*

Under ideal conditions analytes will move through the column without diffusional migration. But, under real conditions analyte diffusion occurs resulting in the spreading of the analyte bands (Figure 1.4). In column chromatography this spreading is called band broadening. An important goal in liquid chromatography is to produce sharp, symmetric, and well resolved peaks as these factors aid in a more accurate calculation of peak area. The sharpness of the chromatographic peaks represent the efficiency of the chromatographic column or, more correctly, the entire chromatographic system [50]. An increase in band broadening results in a decrease in column efficiency by reducing the sharpness of the analyte peak. Therefore, efficiency can be used as a measure of the broadening of the sample zone as it passes through the chromatographic system [50].

The theoretical plate number  $N$  is a measure of column efficiency, where  $t_r$  is the

$$N = 5.54 \left[ \frac{t_r - t_m}{w_{h/2}} \right]^2 \quad (1.18)$$

analyte retention time,  $t_m$  is the system dead time, and  $w_{h/2}$  is the analyte peak width at one-half the peak height. As shown in Figure 1.5, all of these variables are easily obtained from the chromatogram. For the same chromatographic system the column

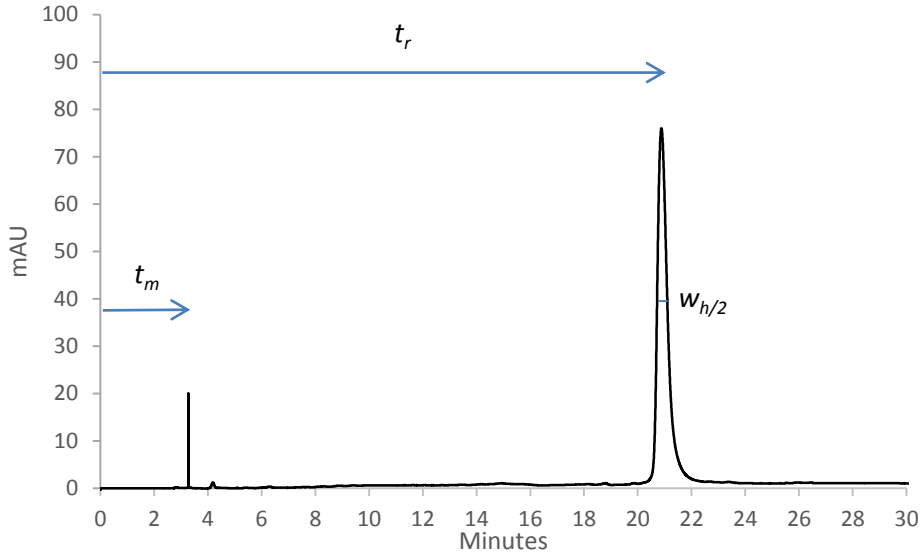


**Figure 1.5** Liquid chromatogram showing dead time,  $t_m$ , analyte retention time,  $t_r$ , and peak width at one-half peak height,  $w_{h/2}$ .

efficiency  $N$  is a function of the column length. Since column length is not directly defined in Eq. (1.18), comparing column efficiency for two columns of different length or type becomes difficult. To describe the relation between column efficiency and column length a new parameter is defined.

$$HETP = \frac{L}{N} \quad (1.19)$$

This parameter, known as the theoretical plate height  $HETP$ , combines a measurement of column length  $L$  with column efficiency  $N$ . Since column length is now defined as a

variable, *HETP* is commonly used to compare columns of different size or stationary phase type.

### *Plate Theory*

Two theories exist that attempt to describe the chromatographic process and its relation to column efficiency. The first theory, called plate theory, describes the chromatographic process analogous to a distillation column. As with a distillation column, this theory describes the chromatographic system as a series of stages or theoretical plates. At each stage analyte equilibrium occurs between two phases. In distillation this is called vapor/liquid equilibrium. In liquid chromatography this is the analyte equilibrium established between the stationary and mobile phases. Plate theory uses Eq. (1.19) to measure column efficiency. The largest shortcoming of plate theory is its failure to relate column efficiency to chromatographic variables such as stationary phase particle size and mobile phase flow rate. [50] While plate theory has been criticized because of this defect it none the less still provides an easily calculated and useful parameter to measure column efficiency.

### *Rate Theory*

Since plate theory suffers from the failure to relate column efficiency to important chromatographic variables, a second theory based on kinetic characteristics was developed. This theory, called rate theory, attempts to relate band broadening to the

*HETP* using a kinetic model. This model focuses on the contribution of various kinetic parameters to the band broadening concept.

$$HETP = A + \frac{B}{u} + C \quad (1.20)$$

Equation (1.20) is the van Deemter equation, written as the sum of three contributing terms to the *HETP*. In this form of the equation,  $u$  is the mobile phase average linear velocity, the  $A$  term represents the contribution to band broadening from eddy diffusion, the  $B$  term represents the contribution from longitudinal diffusion, and the  $C$  term represents the contribution from resistance to mass transfer within the two phases.

#### *Van Deemter Plot*

From an analysts point of view, probably the most useful concept is a combination of both plate and rate theories. Calculation of *HETP* using rate theory, Eq. (1.20), is not trivial, but rate theories relation of *HETP* to the mobile phase velocity is insightful since mobile phase flow rate is a variable that can be optimized to a particular chromatographic analysis. Plate theory uses a simple calculation of *HETP*, Eq. (1.19), using parameters obtained directly from the chromatogram. Therefore, in chromatogram parameter optimization analysts typically use a combination of both theories in the construction of a graph known as the van Deemter plot. [51, 49] The van Deemter plot is a graph of plate height as a function of mobile phase linear velocity or mobile phase flow rate (Figure 1.6).

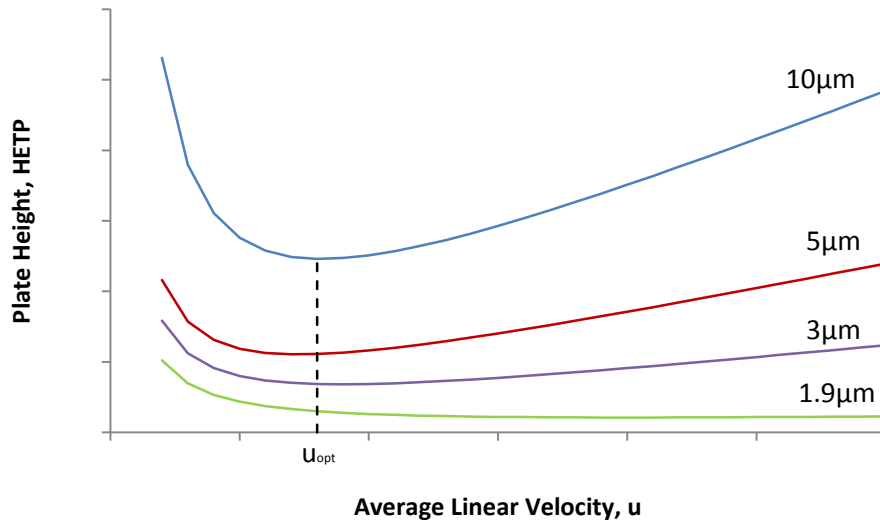


**Figure 1.6** Hypothetical Van Deemter plots for various stationary phase particle sizes.

The graph shown in Figure 1.6 is a van Deemter plot constructed by calculating *HETP* using Eq. (1.19) then graphing *HETP* as a function of mobile phase velocity. Shown in Figure 1.6 for the 10  $\mu\text{m}$  curve, this curve passes through an optimum average linear mobile phase velocity,  $u_{opt}$ , at which *HETP* is at a minimum. Since analysis time is proportional to mobile phase velocity, it is common for analysts to operate at mobile phase velocities greater than the optimum [50, 52]. By operating at greater velocities analysis time is reduced resulting in faster data acquisition, lower mobile phase consumption, and reduced operator time. [49]

Additional efforts to reduce analysis time without sacrificing separation efficiency may be determined by comparing van Deemter plots as a function of stationary phase particle size. [53, 54] The hypothetical van Deemter plots in Figure 1.6 show the relation between particle size, optimum mobile phase flow rate, and *HETP*. As shown, a decrease



in stationary phase particle size results in a reduced effect of mobile phase velocity on *HETP*. This is represented by a curve of lower slope at greater mobile phase velocities. Also, a decrease in *HETP* (i.e. an increase in column efficiency) is typically observed as particle size decreases (Figure 1.6). These effects have been attributed to a solute experiencing a shorter diffusion path length while within the stationary phase particle. [55] This shorter path length results in less time spent within the stationary phase particle where band broadening occurs. Analysts use this relation between particle size and column efficiency to reduce analysis time and increase sample throughput. [56, 57] Due to the increase in column efficiency with the use of smaller particles, shorter columns can be used. [58] Also, smaller particles allow the separation to be performed at higher mobile phase flow rates. By combining a shorter column operating at a greater flow rate, analysis time is significantly reduced resulting in increased sample throughput without a loss in efficiency.

#### 1.3.4 High Performance Liquid Chromatography

High Performance Liquid Chromatography (HPLC) is a derivative of liquid chromatography that operates at high pressure. The HPLC system is composed of: solvent delivery pumps, sample injection system, chromatography column, detector, and a computer that controls all operations (Figure 1.7).

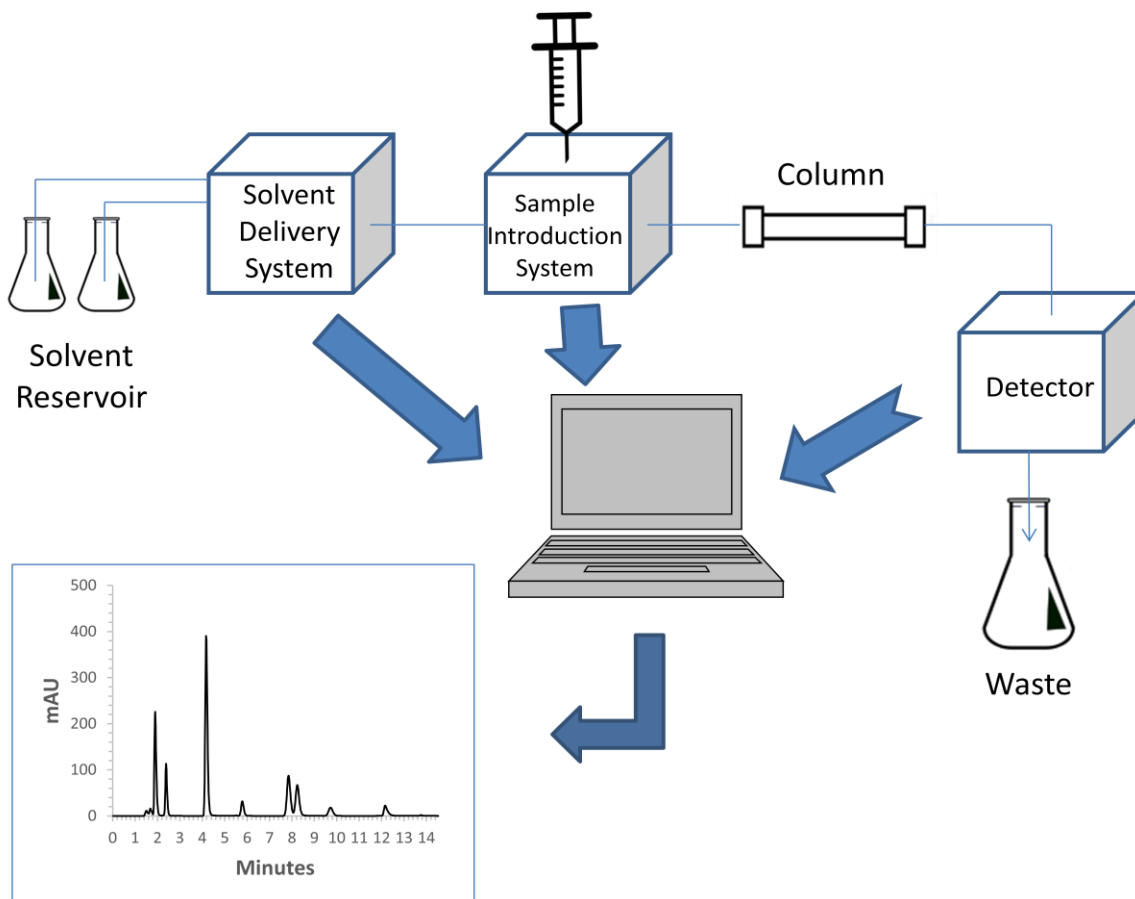


**Figure 1.7** Schematic diagram of an HPLC system.

First, using a high pressure pump solvent from the solvent reservoir is pumped to a sample introduction system. In the sample introduction system, the sample to be analyzed is injected into the solvent flow path and transferred to the inlet of a chromatography column. The chromatography column separates the sample into its different components that individually exit the column. From the column outlet the components enter a detector before finally traveling to a waste container. From the detector a signal is sent to a computer where the chromatogram is generated.

### *Solvent Delivery System*

The primary function of the solvent delivery system (SDS) is to deliver the mobile phase at a constant flow-rate or pressure. Most commonly the SDS is operated at a constant flow-rate. Many detectors used for HPLC are sensitive to pump pulsations. Therefore, for highly reproducible chromatograms, the construction of the solvent delivery pump must be such that it provides a flow-rate that varies by less than one percent. To aid the pump in providing this level of consistency, many system manufactures include a damper as part of the solvent delivery system. The solvent delivery system for HPLC systems consists of one or more high pressure pumps capable of delivering the mobile phase at backpressures up to 6000 p.s.i. [52] Often the solvent delivery systems consist of two or more pumps, providing the user the ability to operate the chromatographic separation under gradient elution mode. [59, 60, 61, 62]

### *Sample Injection System*

The function of the sample introduction system is to introduce the sample into the chromatography system in such a way as to reduce disturbance of the solvent flow, as this may result in chromatogram baseline disruption. There are two types of sample introduction systems for HPLC instrumentation: manual and automated injection. To perform the injection process both types of injection systems use a sample loop connected to a high-pressure injection valve.

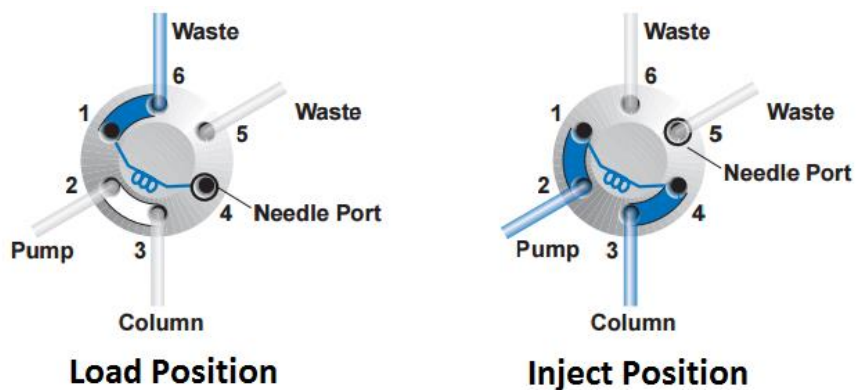


**Figure 1.8** Schematic diagram of Ryeodyne 7725i injection valve in both load and inject positions. Figure modified from reference [63].

The injection procedure begins by rotating the injection valve into the sample load position. In this position the mobile phase bypasses the sample loop and flows directly to the column. Once sample is loaded into the sample loop the injector is rotated to the inject position. In this position the sample loop is placed back into the mobile phase flow path allowing the sample to be transferred to the column inlet.

For manual injection valves loading the sample loop is performed by the analyst using a sample needle specifically designed for the type of manual injector used. During manual sample introduction, to increase precision between samples, the analyst should flush the sample loop with five sample loop volumes before the complete loop volume is injected into the system.

Analytical labs need the ability to program the instrumentation to run numerous samples concurrently without requiring the analyst to inject each sample. Therefore, most HPLC systems used in industry are equipped with an autosampler. The autosampler offers an advantage over manual injector type systems since analyst supervision is

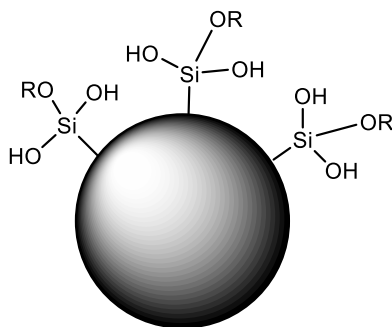
reduced allowing the analyst to concentrate on other laboratory duties. For HPLC systems integrated with an autosampler, sample injection is performed by the instrumentation. First, the analyst fills an autosampler vial with the sample which is then placed into the autosampler carousel. Next, the sample location and sample data are programmed into the HPLC control software. When the run begins the autosampler selects the proper sample, washes the needle with wash solvent followed by a programmed amount of sample, then fills the sample loop, and injects the sample into the mobile phase flow path. The typical sample loop volume installed on an autosampler is 100  $\mu\text{L}$ , but it is more common to inject sample volumes less than 100  $\mu\text{L}$ . Therefore, most autosamplers have the option of a partial sample loop fill mode. Partial sample loop fill mode is the most commonly used sample introduction mode however, using this mode results in a loss in precision when compared to complete fill mode. For complete fill mode the precision is typically in the range of 0.05 to 1% relative standard deviation, while in the partial fill mode precision drops in the range of 0.2 to 2%. [50]

### *Chromatography Column*

The function of the chromatography column is to separate the sample into its individual compounds. Chromatography columns are constructed from a polymer (PEEK) or stainless steel tube packed with a stationary phase. HPLC is a versatile method with the ability to operate in several different types of modes, dependent on the type of stationary phase used. The operational mode is characterized by the relative hydrophobicity of the mobile and stationary phases. The two most common operational

modes are: normal and reverse phase chromatography. Normal phase chromatography is characterized by the stationary phase being less hydrophobic than the mobile phase, while reverse phase mode is characterized as the stationary phase being more hydrophobic than the mobile phase.

In normal phase chromatography the stationary phase is a polar material such as silica gel. Common solvents used in normal phase chromatography are non-polar solvents such as: esters, ethers, alkanes, or chlorinated hydrocarbons. [64] During normal phase chromatography compounds are separated by their dipole interactions with the stationary phase. Therefore, solute compounds that are highly polar will spend a greater proportion of their time on the column within the stationary phase resulting in a longer retention time.

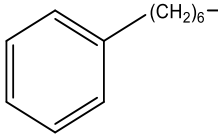
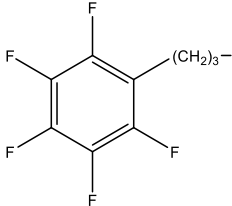
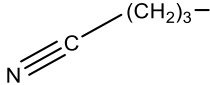
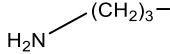


**Figure 1.9** Hypothetical silica stationary phase bead where R is the modified functional group.

In reverse phase chromatography the stationary phase is the same type of silica gel support used in the construction of normal phase columns, but the support has been

functionalized to alter its polarity (Figure 1.9). Typical support alterations include the addition of a C<sub>18</sub>, C<sub>8</sub>, or C<sub>4</sub> hydrocarbon chain to produce siloxane reverse phase packings.

**Table 1.5** Common Types of Modified Silica HPLC Stationary Phases

Functional group name	R=
C <sub>18</sub>	CH <sub>3</sub> -(CH <sub>2</sub> ) <sub>17</sub> -
C <sub>8</sub>	CH <sub>3</sub> -(CH <sub>2</sub> ) <sub>7</sub> -
C <sub>4</sub>	CH <sub>3</sub> -(CH <sub>2</sub> ) <sub>3</sub> -
Phenyl-Hexyl	
Pentafluorophenyl (PFP)	
Cyanopropyl	
Amino	

With such a large assortment of stationary phases commercially available (Table 1.5), an analyst can alter the selectivity of a given separation by simply changing the type of stationary phase used. [62, 65, 66, 67] This ability to alter selectivity results in enhanced flexibility for reverse phase chromatography compared to normal phase

operation. For this reason reverse phase mode is the most widely used of all liquid chromatographic modes.

### *Detectors*

The function of the detector is to monitor the chromatographic run and output a signal to the control computer for the construction of the chromatogram. Due to the use of computer control, an advantage of HPLC is its ability to be connected to various types of detectors. Typical HPLC detectors include the UV-VIS, diode array, fluorescence, and mass spectrum detectors. The two most common HPLC detectors are the UV-VIS and diode array detector.

The HPLC UV-VIS detector operates by the same principals as a common UV-VIS spectrometer. For a UV-VIS spectrometer light intensity and concentration are related by the Beer-Lambert Law:

$$A = \epsilon bC \quad (1.21)$$

where A is the absorbance of the sample, b is the optical path length,  $\epsilon$  is the molar extinction coefficient of the solute at the measuring wavelength, and C is the molar concentration of the solute. [50] At a fixed wavelength, the relationship between absorbance and concentration is linear, but this relationship is valid only when truly monochromatic light is used. Most UV-VIS spectrometers and HPLC detectors use a mercury vapor or deuterium lamp as the light source. These light sources are not monochromatic, therefore a slit is used to filter the light into a narrow range of



wavelengths centered on the wavelength of interest. This filtering results in a short range of wavelengths instead of a monochromatic signal. Since the source signal is not monochromatic it is recommended to operate the detector in wavelength regions where  $\epsilon$  changes very little; that is, at maxima, minima, or shoulders in the absorption spectrum of the solute of interest. [50]

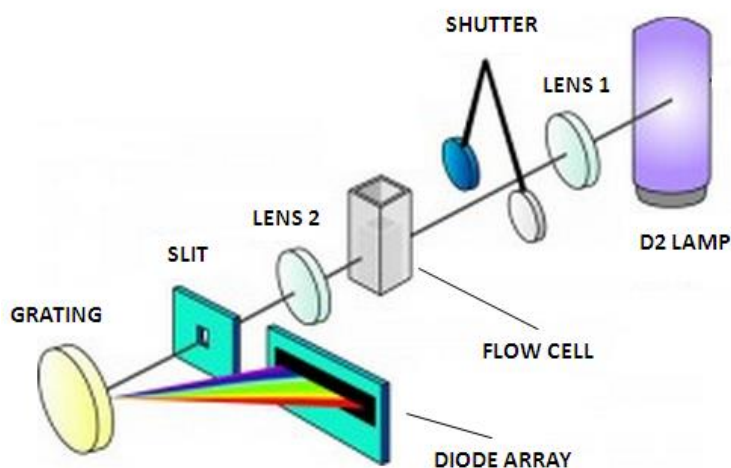


**Figure 1.10** Schematic diagram showing diode-array detector optics. Figure modified from reference [68].

The diode-array detector is an absorption detector capable of simultaneously monitoring all wavelengths between 190 and 800 nm. The arrangement of the optics for a diode array detector is shown in Figure 1.10. From the output of the chromatographic column, the effluent passes through a flow cell. Using a series of lenses polychromatic light from a deuterium lamp is focused onto the flow cell. Light passes through the flow cell and sample to a holographic diffraction grating then is dispersed onto the diode array.

This array consists of several hundred photosensitive diodes configured in a linear pattern which mimics the focal plane of the spectrometer. [50] A capacitor is connected to each diode which is initially charged to a known level. Light falling on the diode discharges the capacitor to a level in relation to the intensity of the light. To generate a chromatogram the signal intensity from each diode in the array is plotted as a function of wavelength and analysis time (Figure 1.11).

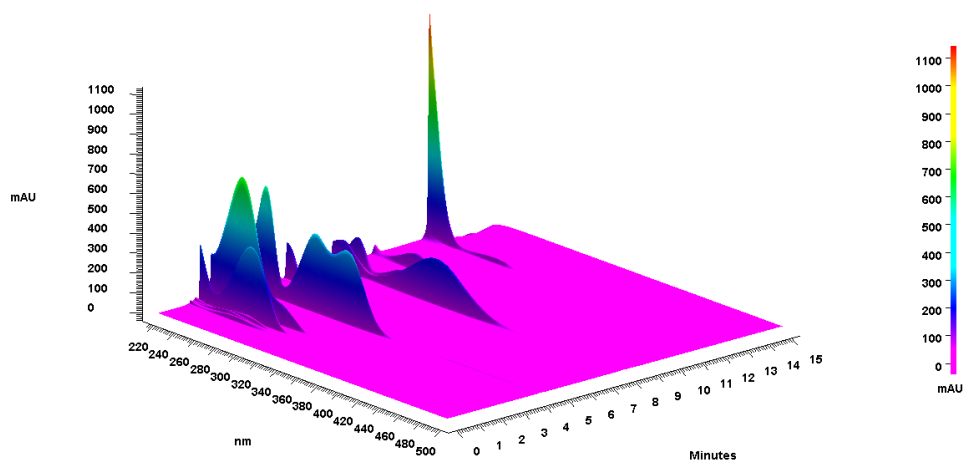


**Figure 1.11** Example chromatogram obtained from an HPLC diode-array detector.

Using this type of detector offers several advantages compared to single wavelength monitoring. For example, the chromatogram can be used to determine peak purity. [50] If a UV-VIS absorbance spectrum of the pure analyte of interest can be obtained, this spectrum can be compared to that obtained from the analyte peak on the diode-array chromatogram. Any differences in relative absorbance may indicate the presence of co-eluting analytes.

## CHAPTER II

### OBJECTIVE

Elastin-like polypeptides (ELPs) are a class of biopolymers with the potential to function as a drug delivery platform. Recently, this class of polymers has been expanded by the addition of a trimer forming oligomerization domain, called foldon, to the C-terminus of an ELP chain (Figure 2.1). [6] The addition of this domain resulted in the development of a three-armed star ELP that has been shown to self assemble into micelles on the nanometer scale when the solution temperature was raised above its transition temperature. [23]

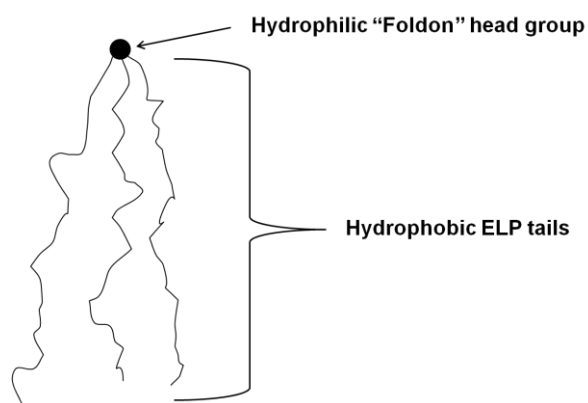


**Figure 2.1** Three-armed star elastin-like polypeptide.

The micellar architecture of this new construct consists of a spherical shape with an outer surface decorated by hydrophilic foldon domains and an interior core consisting of the hydrophobic elastin-like polypeptide (Figure 2.2). Once the micelle core is loaded with therapeutic, these loaded particles potentially have the ability to slowly release the compound from the core into the surrounding environment. [69, 70]

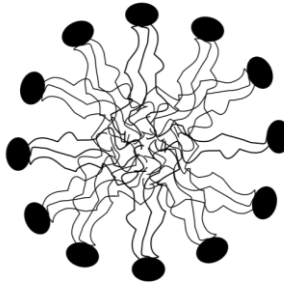


**Figure 2.2** Micelle structure of Foldon-ELP showing micelle core consisting of ELP.

For the use of this micellar construct as a drug delivery platform, solute solubility within the micelle core should be investigated. Information gathered from this study may be used to characterize the micelle interior and determine the required ELP hydrophobicity or amino acid composition necessary for the extended release of therapeutic compounds.

Since the micelle interior consists predominantly of ELP this study uses the coacervate phase of linear ELPs to investigate solute solubility within the micelle core. This investigation is conducted by mixing aqueous solutions of ELP with small molecule

solutes, then the system temperature is raised above the solution transition temperature to cause phase separation. The resulting two-phase system consists of a protein poor upper “supernatant” phase at equilibrium with a lower protein rich “coacervate phase” (Figure 1.1). Next, the phases are separated and solute concentration in each phase is analyzed using high performance liquid chromatography. The partition coefficient of each solute is calculated and reported as the ratio of solute concentration in the protein rich coacervate phase to that of the protein poor supernatant phase.

## **CHAPTER III**

### **MATERIALS AND METHODS**

#### **3.1 Protein Synthesis and Purification**

##### **3.1.1 Protein Synthesis**

All chemicals were purchased from Fisher Scientific. Protein expression media used in this study was Lysogeny Broth (LB). This media was formulated with the composition: 5 g/L yeast extract, 10 g/L peptone, 5 g/L sodium chloride then filled to the required volume using deionized water. Media sterilization was performed using a steam autoclave (Cycle: 121°C for 45 min). The selection agent used in this media was ampicillin at a concentration of 100 mg/L.

Initial protein synthesis was performed on a 1 L expression scale. Since partitioning experiments required between 6 and 18 liters of expression media, protein expression volume was increased to 6 L. The typical protein expression protocol began by preparing a starter culture from LB media inoculated with the appropriate frozen glycerol stock culture. After overnight incubation at 37°C on a shaker table (250 rpm), the starter culture was used to inoculate a larger quantity of LB media. This media was

incubated at 37°C on a shaker table (250 rpm) while monitoring the growth rate using a UV-VIS spectrometer ( $\lambda = 600$  nm). Once the desired cell density ( $OD_{600} = 0.8$  to 1.2) was achieved the culture was induced using isopropyl  $\beta$ -D-1-thiogalactopyranoside (IPTG). Induction was allowed to proceed for a minimum of 5 hours then bacteria were isolated by centrifugation (20°C, 10,000xg, 10 min). A more detailed description of both the 1 L and 6 L expression procedures are outlined in Appendix A.

### 3.1.2 Protein Extraction and Purification

After isolation of the bacteria, the pellet was resuspended in deionized water, cooled in an ice bath below 10°C, and pulse sonicated (550 Sonic Dismembrator, Fisher Scientific) using the pulse sequence of: 10 s on (100% power) then 20 s off while keeping the solution temperature below 10°C. Following sonication the protein was purified by inverse transition cycling (ITC). [71] A typical round of ITC protocol began by cooling the protein solution below 5°C using an ice bath, then centrifuging cold (3°C, 20,000xg, 20 min) to remove insoluble material. Next, the protein solution was decanted from the insoluble material, then the decanted solution temperature was raised to 55°C and held at this temperature for 30 minutes, causing the protein to separate from solution. Finally, the protein pellet was isolated by hot centrifugation (40°C, 20,000xg, 10 min), completing one round of ITC. Typically, three rounds of ITC were performed using the resuspension volumes of 15, 5, and 1 mL/L culture for each subsequent cycle. Occasionally, sodium chloride was added and solution pH was adjusted to aid in protein purification. A complete description of the protein purification procedure is outlined in Appendix B. After protein purification, protein solution purity was determined by

HPLC. Typical solution purity after three rounds of ITC was greater than 95%. Final protein solution concentration was determined by UV-VIS spectroscopy measured at 280 nm using the calculated extinction coefficient (Table 3.1).

**Table 3.1** Amino Acid Sequences for all Proteins Investigated along with their Molecular Weight and Extinction Coefficient at 280 nm

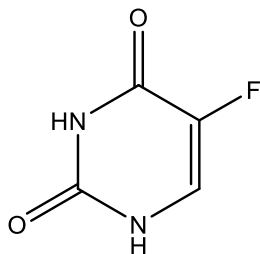
Protein construct	Amino acid sequence	Molecular weight (g/mole)	Extinction coefficient @ 280 nm ( $M^{-1} \text{ cm}^{-1}$ )
(GVGVP) <sub>40</sub>	MGH-(GVGVP) <sub>40</sub> -GWP	17,066	5,500
(LQQ) <sub>12</sub>	MGH-(GLGVP-GQGVP-GQGVP) <sub>12</sub> -GWP	16,290	5,500
(V <sub>3</sub> (VH) <sub>3</sub> ) <sub>4</sub>	MGH-[(GVGVP) <sub>3</sub> -(GVGVP-GHGVP) <sub>3</sub> ] <sub>4</sub>	15,881	5,500

### 3.2 Solutes Investigated

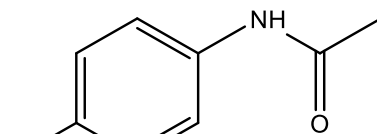
To aid in detection by UV-VIS spectroscopy, the solutes investigated in this study (Figure 3.1) were selected according to two criteria. First, all solutes should have a water solubility greater than or equal to 1 mg/mL and second, all solutes should possess a high extinction coefficient.



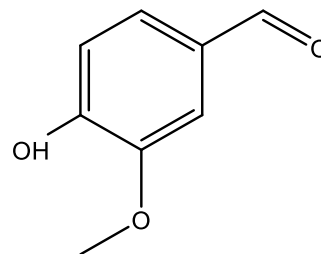
1. 5-Fluorouracil



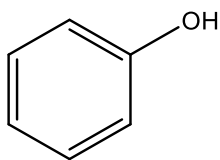
2. Acetaminophen



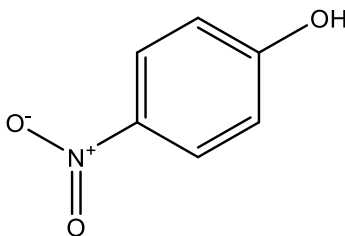
3. Vanillin



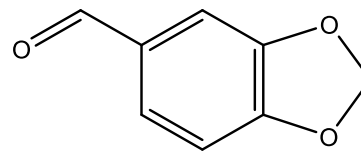
4. Phenol



5. 4-Nitrophenol



6. Piperonal



7. Ethyl Paraben

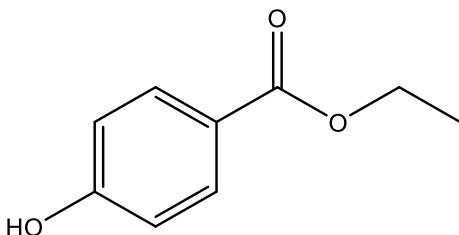


**Figure 3.1** Structures for all compounds investigated in this study.

### 3.3 Master Stock Solute Solution Preparation

A master stock solute solution of the investigated compounds was prepared by dissolving each compound into water at concentrations of approximately 1 to 5 mg/mL. This master stock solute solution was used for all partitioning experiments in this study. The solute compounds 5-fluorouracil, acetaminophen, and 4-nitrophenol were purchased

from Acros Organics. Vanillin, phenol, ethyl paraben, and piperonal were purchased from Alfa Aesar.

### **3.4 Partition Coefficient Calculation Procedure**

The partition coefficient,  $K$ , is defined as the ratio of the solute concentration in the lower coacervate phase to the solute concentration in the upper supernatant phase, Eq. (1.11). To calculate the partition coefficient for each compound a plot of compound peak area in the coacervate phase as a function of compound peak area in the supernatant phase, obtained by HPLC, was constructed. The partition coefficient was determined as the slope of a linear regression line of best fit.

### **3.5 Partitioning**

Partitioning experiments were performed by varying the solute concentration at a fixed protein concentration (1 mM protein concentration) and system temperature (37°C or 55°C). Both PBS (0.15 M NaCl, 0.01 M Na<sub>3</sub>PO<sub>4</sub>, pH 7.4) and water solvent conditions were explored. All experiments were performed in duplicate according to the following procedure.

The partitioning vessel was constructed from a 4 mm inside diameter glass nuclear magnetic resonance (NMR) tube cut to a length of 8.5 cm. Protein solutions were prepared by diluting the desired protein stock solution to a final concentration of 1 mM protein in both 1.08xPBS and water. Each partitioning experiment consisted of

measuring the partition coefficient at four different solute concentrations. Therefore, four of the constructed NMR tubes were numbered and their individual masses measured using a microbalance. After their masses were recorded each tube was charged with 500  $\mu\text{L}$  of the desired 1 mM protein solution. Varying amounts of the master stock solute solution was added (10, 20, 30, and 40  $\mu\text{L}$ ) to each NMR tube followed by the complementary amount (30, 20, 10, and 0  $\mu\text{L}$ ) of water. Next, each tube was sealed, moderately vortexed to ensure a well-mixed solution, then centrifuged for 2 min at 2,000xg and 10-15°C.

Phase separation was performed by placing the tubes in an incubator at a temperature above the solution transition temperature for approximately 18 hours. For protein constructs (GVGVP)<sub>40</sub> and (V<sub>3</sub>(VH)<sub>3</sub>)<sub>4</sub>, the incubator temperature was 37°C; for protein construct (LQQ)<sub>12</sub>, the incubator temperature was 55°C. Once phase separation was complete all tubes were centrifuged (15 min at 2,000xg) at their respective system temperature.

Quickly, before significant cooling of the partitioned system, the top supernatant phase was removed using a glass pasture pipet, ensuring the bottom coacervate phase was not disturbed. After removal of the supernatant phase a cotton swab was used to remove residual supernatant from the wall of the tube. The total mass of the tube containing the coacervate was recorded then 500  $\mu\text{L}$  of deionized water was added to the tube. Once again the total mass of the tube was recorded, then the tube sealed. Finally, the solution was cooled in ice, moderately vortexed to ensure a well-mixed solution, and transferred to an HPLC autosampler vial for analysis.

### 3.6 High Performance Liquid Chromatography Setup

Chromatographic methods were developed by analyzing the master stock solute solution and the desired protein solution separately then as a combined solution. The HPLC system consisted of a two pump solvent delivery module (Beckman Coulter Model: System Gold 126 Solvent Module), an autosampler (Beckman Coulter Model: System Gold 508 Autosampler), and a diode array detector (Beckman Coulter Model: System Gold 168 Detector). The separation was performed on a 250 x 5 mm I.D. (5  $\mu$ m) reverse phase C<sub>18</sub> Luna column (Phenomenex) with guard cartridge (Phenomenex Security Guard). Injection volume was 20  $\mu$ L for all analyses. Mobile phase A composition was water:acetonitrile:trifluoroacetic acid (94.9:5:0.1, v/v/v) and mobile phase B composition was 100% acetonitrile. Column effluent was monitored at a detector wavelength of 280 nm. All chromatograms were collected at room temperature (20°C). Data collection and instrument operation was performed by 32 Karat software (Beckman Coulter). All HPLC mobile phase solvents were of HPLC grade and purchased from Fisher Scientific. Chromatogram optimization was performed in an effort to reduce analysis time while providing well resolved and symmetric solute peaks.

#### 3.6.1 Mobile Phase Gradient Profile for the (GVGVP)<sub>40</sub> Protein System

The mobile phase profile (Figure 3.2-A) for protein system (GVGVP)<sub>40</sub> started with a mobile phase composition of 32% B. This composition was held for 8 minutes then increased to 55% B. After 3.5 minutes at 55% B the column was re-equilibrated at

32% B for 3 minutes. Throughout the separation the mobile phase flow rate was maintained constant at 1.5 mL/min. Total run time including re-equilibration period was 14.5 minutes.

### 3.6.2 Mobile Phase Gradient Profile for (LQQ)<sub>12</sub> Protein System

For protein system (LQQ)<sub>12</sub> separation (Figure 3.2-B) was accomplished starting at an initial mobile phase composition of 10% B. After holding at 10% B for 1.5 minutes the mobile phase composition was increased to 35% B followed by a linear gradient to 40% B ending at 7 minutes. The composition was held for 3 minutes at 40% B then re-equilibrated for 3 minutes at 10% B. Mobile phase flow rate was held constant at 1.5 mL/min. Total run time including re-equilibration was 13 minutes.

### 3.6.3 Mobile Phase Gradient Profile for (V<sub>3</sub>(VH)<sub>3</sub>)<sub>4</sub> Protein System

Mobile phase composition (Figure 3.2-C) started at 15% B with a linear gradient programmed to increase composition to 50% B over 6 minutes. Composition was held at 50% B for 4 minutes then system was re-equilibrated for 3 minutes at 15% B. Mobile phase flow rate was held constant at 1.0 ml/min. Total run time including re-equilibration period was 13 minutes.

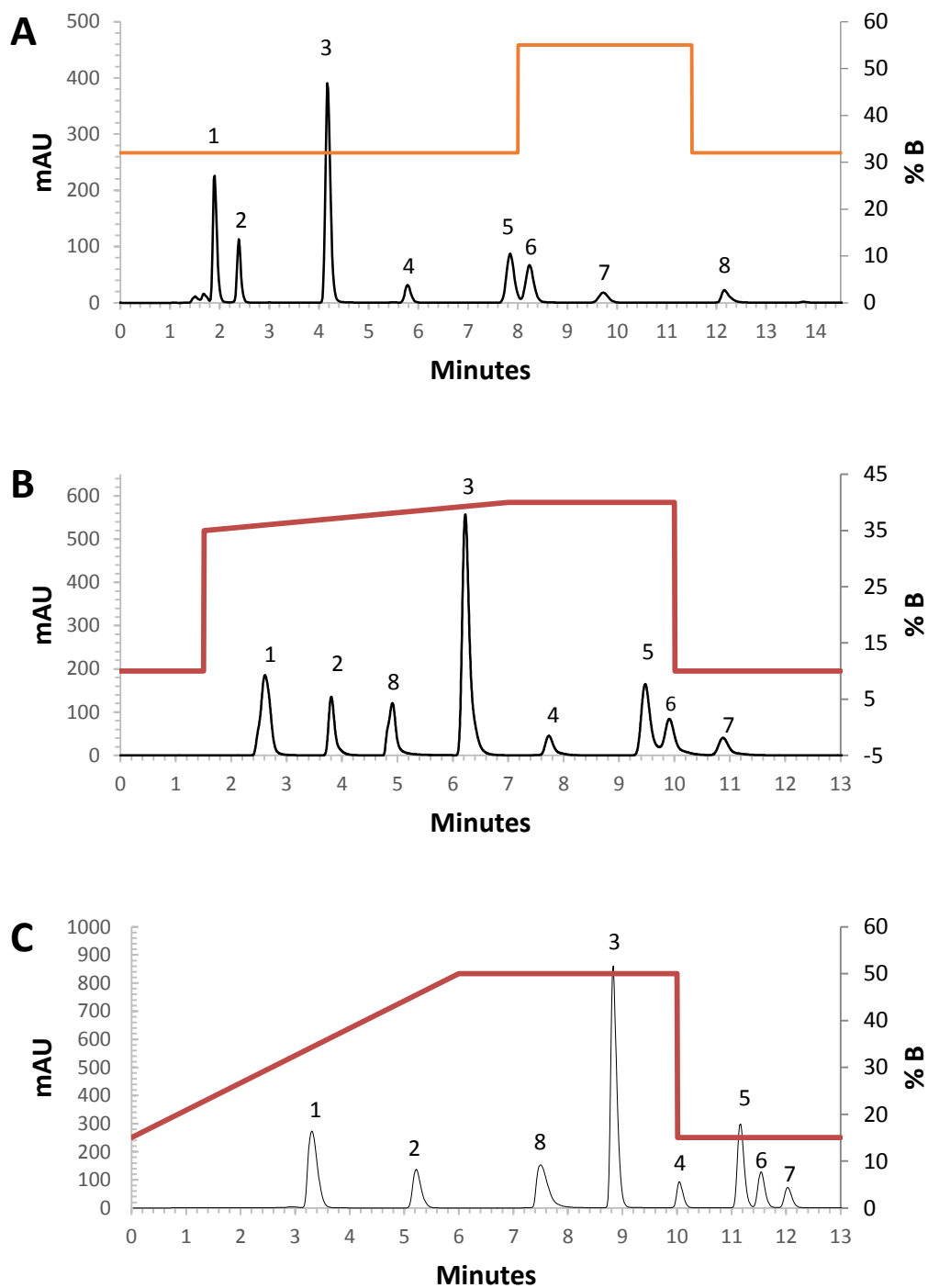


**Figure 3.2** Representative chromatograms and gradient profiles for solvent/protein systems: A. (GVGVP)<sub>40</sub>, B. (LQQ)<sub>12</sub>, and C. (V<sub>3</sub>(VH)<sub>3</sub>)<sub>4</sub>. Solutes: (1) 5-fluorouracil, (2) acetaminophen, (3) vanillin, (4) phenol, (5) 4-nitrophenol, (6) piperonal, (7) ethyl paraben, and (8) respective protein.

## CHAPTER IV

### RESULTS AND DISCUSSION

The partition coefficient,  $K$ , of a solute is defined as the ratio of solute concentrations between two phases at equilibrium. Equation (4.1) shows the octanol/water partition coefficient where  $[\text{Solute}]$  is the solute concentration and the subscript 'o' and 'w' represent the composition of the respective phase.

$$K_{o/w} = \frac{[\text{Solute}]_o}{[\text{Solute}]_w} \quad (4.1)$$

In this study partition coefficients were determined for solvent systems composed of a protein rich coacervate (co) and protein poor supernatant phase (sn). To keep the identical nomenclature as the octanol/water partitioning system, the partition coefficients measured in the investigated protein systems were defined as the ratio where the more water rich phase is the denominator, Eq. (4.2).

$$K_{co/sn} = \frac{[\text{Solute}]_{co}}{[\text{Solute}]_{sn}} \quad (4.2)$$

Since the solute peak area is proportional to concentration, solute calibration was not necessary. When calculating the partition coefficients solute peak areas were used instead of solute concentrations, Eq. (4.3). Two requirements are necessary to use peak area (or signal) from a detector as a replacement for concentration. First, one must verify that solute peak area is linearly proportional to concentration over the range of interest and second, the intercept of the calibration curve used for detector signal to concentration conversion must be set to zero. When these requirements are met, the slope of the calibration curve ‘m’ will cancel out of the equation during the calculation of ‘K’ leaving only the ratio of detector signals, Eq. (4.3).

$$K_{co/sn} = \frac{(\#)*[Solute]_{co}}{(\#)*[Solute]_{sn}} = \frac{\text{Solute peak area in coacervate}}{\text{Solute peak area in supernatant}} \quad (4.3)$$

To check for detector linearity 11 concentrations of the master solute stock solution were analyzed by HPLC using the mobile phase gradient profile for (GVGVP)<sub>40</sub>. Linear regression was performed with the intercept set at zero then the correlation coefficient (r<sup>2</sup>) and slope were calculated (Table 4.1, Appendix C).

**Table 4.1** Results from HPLC DAD Detector Linearity Check at 280 nm Wavelength

Compound	Slope (10 <sup>5</sup> )	r <sup>2</sup>	Lowest Standard Area (10 <sup>3</sup> )	Highest Standard Area (10 <sup>6</sup> )
5-Fluorouracil	3.3	1.00	5.3	6.6
Acetaminophen	1.7	1.00	2.7	3.3
Vanillin	7.9	1.00	9.8	16
Phenol	0.8	1.00	1.5	1.6
4-Nitrophenol	3.0	1.00	3.6	5.9
Piperonal	2.7	1.00	4.2	5.3
Ethyl paraben	0.8	1.00	3.6	1.7



The correlation coefficient for all compounds shows a strong linear correlation between concentration and detector signal over the range investigated. This result suggests using HPLC peak areas is a valid replacement for concentration to calculate partition coefficients.

After phase separation HPLC was used to measure solute peak area in the supernatant and coacervate phases. The supernatant phase could be analyzed by HPLC without any further sample preparation, but since the coacervate phase volume was only 10-15  $\mu\text{L}$  and the phase viscosity is like that of room temperature honey, dilution of the coacervate phase was necessary before analysis. Since the coacervate phase was diluted, it was necessary to record the initial coacervate mass and the final solution mass to back calculate the peak area in the undiluted coacervate, Eq. (4.4) and (4.5). Since this

$$\text{Solute peak area in coacervate} = \frac{(\text{Solute peak area in diluted coacervate})}{\Gamma} \quad (4.4)$$

$$\text{Coacervate mass fraction} = \Gamma = \frac{\text{Coacervate mass}}{\text{Final solution mass}} \quad (4.5)$$

procedure involves the measuring of a small mass difference (i.e. the difference between the NMR tube with and without coacervate), it is possible that this procedure is more susceptible to error. For example, the data presented in Table 4.2 are the measured masses of coacervate in milligrams for one partition experiment consisting of four sample tubes. A high percent relative standard deviation (%RSD) is shown in the original data suggesting a large range in the measured values. While this range could possibly be due to errors in experimental procedure, each sample tube was originally charged with an identical volume of the same protein solution. Therefore, it is more likely that the high %RSD may be the result from error in one or both of the mass measurements used in the

calculation of the solute peak area in the coacervate. Figure 4.1 is a plot of the solute peak area in the coacervate as a function of solute peak area in the supernatant for the

**Table 4.2** Measured Coacervate Masses for  $(V_3(VH)_3)_4$  protein system with PBS

Sample Tube #	1	2	3	4	Average	%RSD
Original CO wt (mg)	16.5	17.1	14.1	15.5	15.8	8.3
Distance from Average (mg)	0.7	1.3	1.7	0.3		

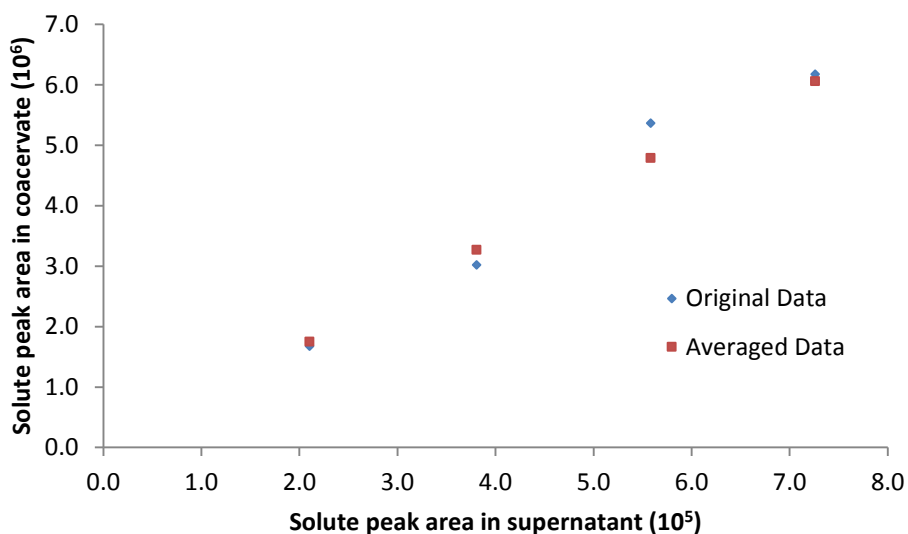


**Figure 4.1** Plot of original data and averaged coacervate mass data for ethyl paraben in the  $(V_3(VH)_3)_4$  protein system with PBS.

solute compound ethyl paraben. As shown, in the original data the third data point does not follow the linear trend observed for all other data points in its series. Since all sample tubes were charged with approximately the same volume of protein stock solution an average of the coacervate masses was used to recalculate the peak areas. This resulted in

a better linear trend in the data suggesting error in the mass measurement is responsible for the variance in the original data. Errors associated with the mass measurements also had an effect on the partition coefficient and its 95% confidence interval. In the original data the partition coefficient for this solute was 9.21 with a confidence interval of 4.66. In the average adjusted data the partition coefficient and confidence interval were reduced to 8.38 and 0.92 respectively.

To reduce measurement error an alternative method of calculating the solute peak area in the coacervate phase was explored. This method utilizes the measured protein peak area in the coacervate sample along with the GRG nonlinear equation solver tool in Microsoft Excel to calculate the original coacervate mass. The equation derivation begins with Eq. (4.4) and (4.5). In the previous calculation method the coacervate mass fraction ' $\Gamma$ ' was calculated using the measured masses of both the final solution mass and coacervate mass. In this method the coacervate mass fraction was determined by relating the mass fraction to the protein peak area (Figure 4.2).

Figure 4.2 is a plot of  $(GVGVP)_{40}$  coacervate mass fraction as a function of protein peak area for 3 different sets of data measured at different times. The difference in slope is attributed to the change in detector response at the time of analysis. The purpose of Figure 4.2 is only to show how the slope changes between analyses. In practice the slope from Figure 4.2 was not used in the calculation, but instead calculated as the correction factor ' $\zeta$ '.

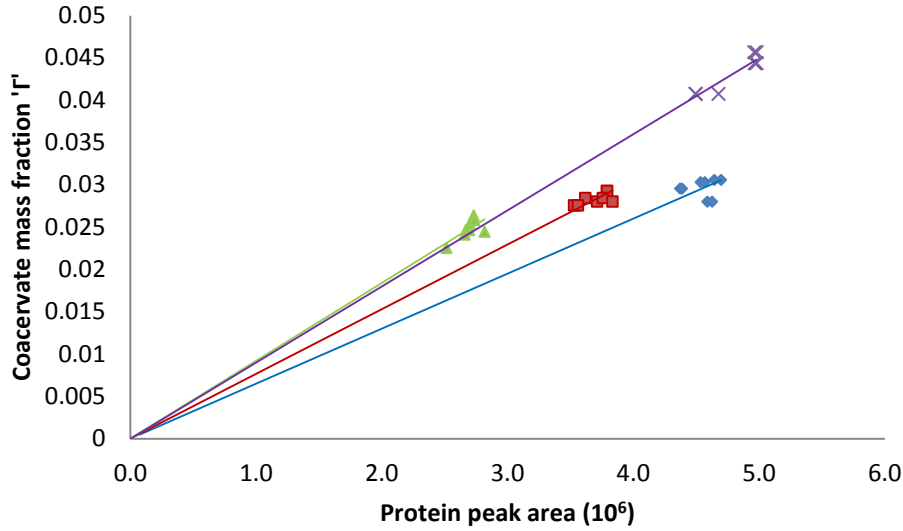


**Figure 4.2** Plot of coacervate mass fraction as a function of (GVGVP)<sub>40</sub> protein peak area for several data sets.

Based upon the concept represented in Figure 4.2, Eq. (4.6) relates the protein peak area in the diluted coacervate sample to the coacervate mass fraction.

$$\Gamma = (\xi)(\text{Protein peak area in diluted coacervate}) \quad (4.6)$$

By combining Eq. (4.4) and (4.6), Eq. (4.7) calculates the undiluted solute peak area from the diluted solute peak area and the protein peak area.

$$\text{Solute peak area in coacervate} = \frac{(\text{Solute peak area in diluted coacervate})}{(\xi)(\text{Protein peak area in diluted coacervate})} \quad (4.7)$$

The final equation, Eq. (4.8), used for calculating the partition coefficient of a solute was derived by combining Eq. (4.3) and (4.7).

$$K_{\text{co/sn}} = \frac{(\text{Solute peak area in diluted coacervate})}{(\xi)(\text{Protein peak area in diluted coacervate})(\text{Solute peak area in supernatant})} \quad (4.8)$$

In Eq. (4.8) all variables are obtained from the chromatogram except for the correction factor ‘ $\xi$ ’. This value was obtained iteratively using the procedure below.

- To obtain the value of ‘ $\xi$ ’ a reference solute was established. For this study the reference solute was 5-fluorouracil.
- The partition coefficient of the reference solute was calculated using Eq. (4.3), (4.4), and (4.5).
- The Microsoft Excel GRG nonlinear equation solver was setup by fixing the target cell to the partition coefficient of the reference solute then changing the value of ‘ $\xi$ ’ such that it satisfies Eq. (4.8).

This value of ‘ $\xi$ ’ was then used to determine all remaining solute partition coefficients for that set of data. Since the slope of Eq. (4.6) is not a constant (Figure 4.2) a new value of ‘ $\xi$ ’ was calculated for each data set. Results from using both the coacervate mass and protein peak area calculations are shown in Table 4.3 for the (GVGVP)<sub>40</sub> protein solvent system. Sample graphs for the two methods of calculation are presented in Figure 4.3.

The results show the 95% confidence interval for all partition data using the protein peak area was narrower than that obtained from using the coacervate mass calculation (Table 4.3). Since the confidence interval is narrower using the protein peak area method all further protein systems were evaluated using this method of calculation (Table 4.4).

**Table 4.3** Comparison of Partition Coefficients and 95% Confidence Interval using the Coacervate Mass and Protein Peak Area Methods of Calculation

ELP Type	Solute	Calculation Method	
		Coacervate Mass	Protein Peak Area
(GVGVP) <sub>40</sub>	5-Fluorouracil	1.03 (0.04)	1.02 (0.03)
	Acetaminophen	4.66 (0.28)	4.54 (0.14)
	Vanillin	5.32 (0.29)	5.12 (0.14)
	Phenol	5.58 (0.43)	5.01 (0.41)
	4-Nitrophenol	5.63 (0.31)	5.42 (0.09)
	Piperonal	6.57 (0.28)	6.37 (0.18)
	Ethyl paraben	15.1 (1.2)	14.2 (0.2)

95% Confidence interval displayed in parentheses

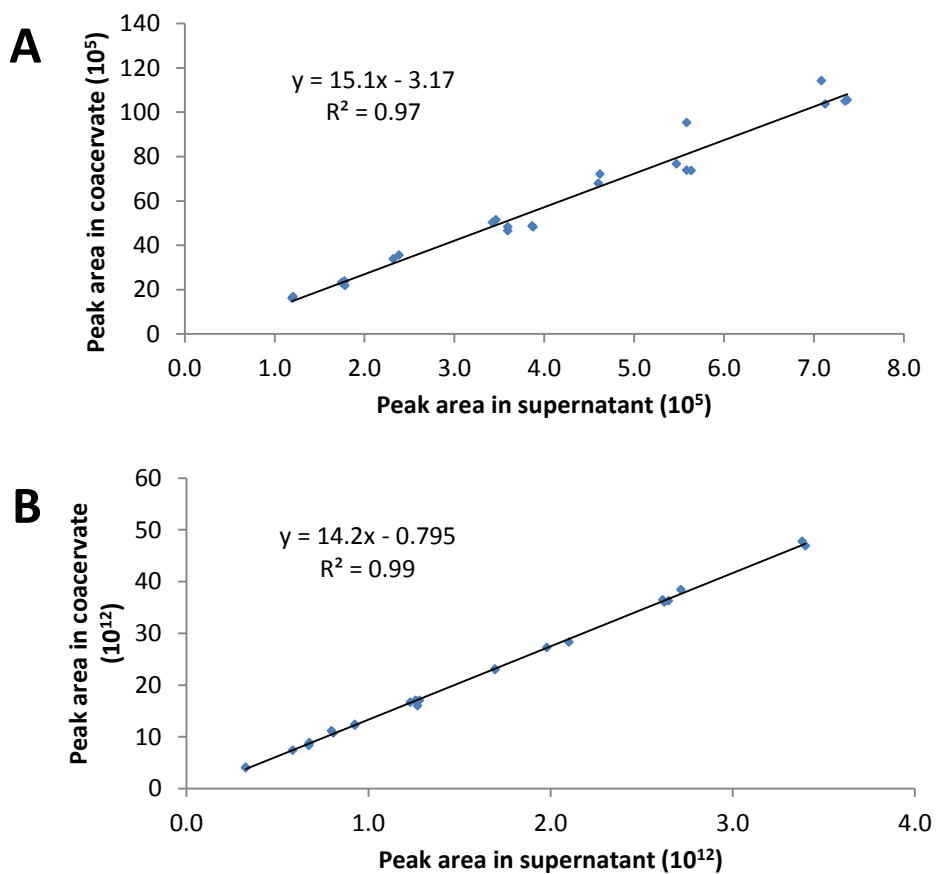


**Figure 4.3** Example results from (A) using coacervate mass and (B) protein peak area for calculation. Solute was ethyl paraben in solvent system (GVGVP)<sub>40</sub> with PBS.

**Table 4.4** Final Results Table Displaying Partition Coefficients of Several Solutes in 5 Protein/Solvent Two-Phase Systems

ELP Type	Solute	Composition				n
		Deionized water		PBS pH 7.4		
		K(co/sn)		K(co/sn)		
<b>(GVGVP)<sub>40</sub></b>	<b>5-Fluorouracil</b>	1.18	(0.06)	1.02	(0.03)	24
	<b>Acetaminophen</b>	3.88	(0.18)	4.54	(0.14)	24
	<b>Vanillin</b>	5.65	(0.28)	5.12	(0.14)	24
	<b>Phenol</b>	3.80	(0.27)	5.01	(0.41)	24
	<b>4-Nitrophenol</b>	7.85	(0.44)	5.42	(0.09)	24
	<b>Piperonal</b>	4.73	(0.25)	6.37	(0.18)	24
	<b>Ethyl paraben</b>	12.2	(0.6)	14.2	(0.2)	24
<b>(V<sub>3</sub>(VH)<sub>3</sub>)<sub>4</sub></b>	<b>5-Fluorouracil</b>	1.18	(0.78)	1.21	(0.13)	16
	<b>Acetaminophen</b>	2.22	(0.64)	3.91	(0.22)	16
	<b>Vanillin</b>	3.70	(0.73)	4.43	(0.24)	16
	<b>Phenol</b>	1.69	(1.57)	4.09	(0.27)	16
	<b>4-Nitrophenol</b>	5.10	(0.34)	5.02	(0.26)	16
	<b>Piperonal</b>	2.54	(0.57)	5.04	(0.26)	16
	<b>Ethyl paraben</b>	4.82	(0.62)	9.75	(0.51)	16
<b>(LQQ)<sub>12</sub></b>	<b>5-Fluorouracil</b>			1.08	(0.04)	8
	<b>Acetaminophen</b>			2.21	(0.32)	8
	<b>Vanillin</b>			4.33	(0.83)	8
	<b>Phenol</b>			4.77	(0.62)	8
	<b>4-Nitrophenol</b>			2.94	(0.79)	8
	<b>Ethyl paraben</b>			5.14	(0.35)	8

95% Confidence interval displayed in parentheses

n is the number of data points used for data regression

To further investigate the solvent phases, solvent descriptors were calculated based on the linear free energy relationship described by Abraham, Eq. (4.9).

$$\log(K) = eE + sS + aA + bB + vV + c \quad (4.9)$$

This equation models five interaction parameters where E, S, A, B, and V are solute descriptors and e, s, a, b, v, and c are solvent descriptors. To calculate the solvent

descriptors, the measured partition coefficients and the solute descriptors, obtained from literature (Table 4.5), were combined to generate six equations with the six solvent descriptors as unknowns. These six equations were then solved for the solvent descriptors by minimizing an objective function, Eq. (4.10). The calculated solvent descriptors serve to characterize the solvent system under investigation and in the case where the LFER describes a partitioning process, such as Eq. (4.9), the solvent descriptors represent the difference in properties of the two phases taking part in the partitioning process. [72]

$$\text{objective function} = \sum(\log(K)_{\text{fit}} - \log(K)_{\text{exp}})^2 \quad (4.10)$$

**Table 4.5** Literature Values of Solute Descriptors

Solute	Solute Descriptors					Ref.
	E	S	A	B	V	
<b>5-Fluorouracil</b>	0.72	0.84	0.57	1.02	0.7693	[38]
<b>Acetaminophen</b>	1.06	1.63	1.04	0.86	1.1724	[73]
<b>Vanillin</b>	0.99	1.30	0.31	0.68	1.1313	[33]
<b>Phenol</b>	0.805	0.89	0.6	0.3	0.7751	[73]
<b>4-Nitrophenol</b>	1.07	1.72	0.82	0.26	0.9493	[73]
<b>Ethyl Paraben</b>	0.91	1.44	0.73	0.45	1.2722	[74]



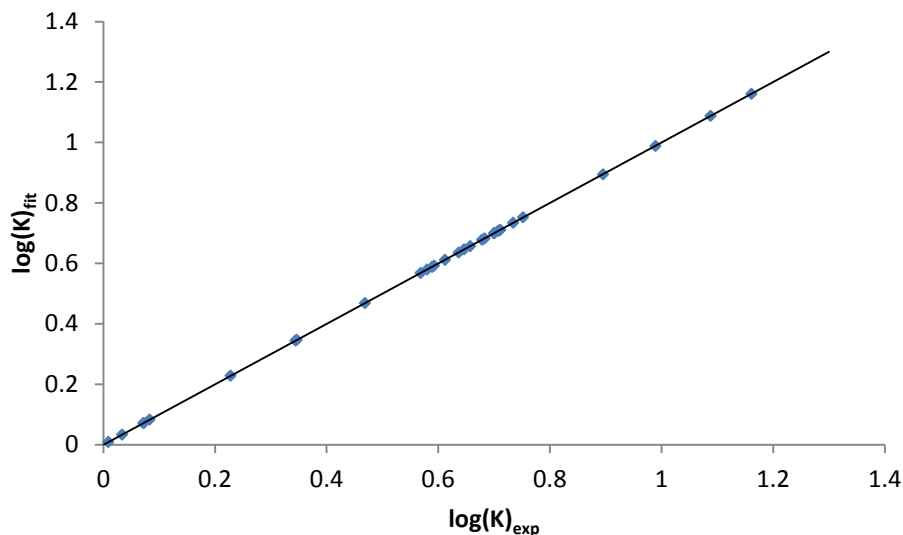


**Figure 4.4**  $\log(K)_{\text{fit}}$  as a function of  $\log(K)_{\text{exp}}$  using all interaction parameters for calculation.

**Table 4.6** Calculated Solvent Descriptor using all Interaction Parameters

Solvent	Solvent Descriptors					
	e	s	a	b	v	c
$(\text{GVGVP})_{40} + \text{PBS}$	0.471	-0.572	0.276	-0.919	1.646	-0.336
$(\text{V}_3(\text{VH})_3)_4 + \text{PBS}$	0.169	-0.271	0.141	-0.718	1.203	-0.085
$(\text{LQQ})_{12} + \text{PBS}$	1.625	-1.054	0.047	-0.766	1.107	-0.348
$(\text{GVGVP})_{40}$	-0.663	0.400	-0.211	-0.757	1.003	0.333
$(\text{V}_3(\text{VH})_3)_4$	-1.351	1.106	-0.608	-0.323	0.234	0.612

As expected, since the number of adjustable parameters was equal to the number of solutes, using all interaction descriptors resulted in perfect agreement between the calculated fit and experimental  $\log(K)$  values (Figure 4.4, Table 4.6). For a more accurate solvent descriptor calculation it has been suggested to solve the system of equations in an over-determined condition by using a larger number of solutes than the number of adjustable parameters. [41] Therefore, a series of calculations were performed

eliminated one interaction descriptor at a time and recording the value of the objective function (Table 4.7).

**Table 4.7** Objective Function Value when Interaction Descriptor was Eliminated from Linear Free Energy Equation

Solvent	Eliminated Interaction Descriptor				
	eE	sS	aA	bB	vV
(GVGVP) <sub>40</sub> + PBS	1.43E-03	1.08E-02	1.02E-02	3.31E-01	2.53E-01
(V <sub>3</sub> (VH) <sub>3</sub> ) <sub>4</sub> + PBS	2.39E-04	2.57E-03	2.69E-03	1.99E-01	1.32E-01
(LQQ) <sub>12</sub> + PBS	2.22E-02	3.87E-02	2.98E-04	2.27E-01	1.12E-01
(GVGVP) <sub>40</sub>	3.69E-03	5.59E-03	5.97E-03	2.21E-01	9.16E-02
(V <sub>3</sub> (VH) <sub>3</sub> ) <sub>4</sub>	1.54E-02	4.26E-02	4.96E-02	4.02E-02	4.99E-03

Smallest values for each solvent system shown in yellow, largest in green.

The results of this procedure show that for the four protein systems, (GVGVP)<sub>40</sub>, (GVGVP)<sub>40</sub> + PBS, (V<sub>3</sub>(VH)<sub>3</sub>)<sub>4</sub> + PBS, and (LQQ)<sub>12</sub> + PBS, the 'bB' and 'vV' interaction descriptors are the most influential of all interaction types. This indicates that solute basicity and its interaction with solvent acidity, along with the solute size and solvent dispersive interaction strength are important interactions in these systems. For the (V<sub>3</sub>(VH)<sub>3</sub>)<sub>4</sub> system the most important interactions arise from those between solute acidity and solvent basicity 'aA' along with solvent polarizability and dipolar interactions 'sS'.

For all the protein systems the results in Table 4.7 show that no single interaction descriptor had the least impact on the objective function. To compare solvent systems with and without the addition of PBS it is necessary to compare systems with the same interaction descriptors. Since the 'eE' interaction descriptor had the least impact on the

objective function for the most solvent systems ((GVGVP)<sub>40</sub> + PBS, (V<sub>3</sub>(VH)<sub>3</sub>)<sub>4</sub> + PBS, and GVGVP)<sub>40</sub>) and the second least impact for the two remaining systems ((V<sub>3</sub>(VH)<sub>3</sub>)<sub>4</sub> and (LQQ)<sub>12</sub> + PBS) this interaction descriptor was excluded. While this excluded descriptor had little effect on the objective function for the solute/solvent combinations investigated, it is probable that it will become more important as different types of solutes and solvents are investigated, but for these solute/solvent combinations, this interaction descriptor was eliminated to provide an over-determined condition and then the solvent descriptors were recalculated (Figure 4.5, Table 4.8).

Equation (4.11) shows the LFER equation format for the (GVGVP)<sub>40</sub> + PBS protein system and describes the respective solvent system where N is the number of solutes during data fitting, R<sup>2</sup> is the adjusted correlation coefficient, SE is the standard error in the dependent variable, and F is the fisher statistic.

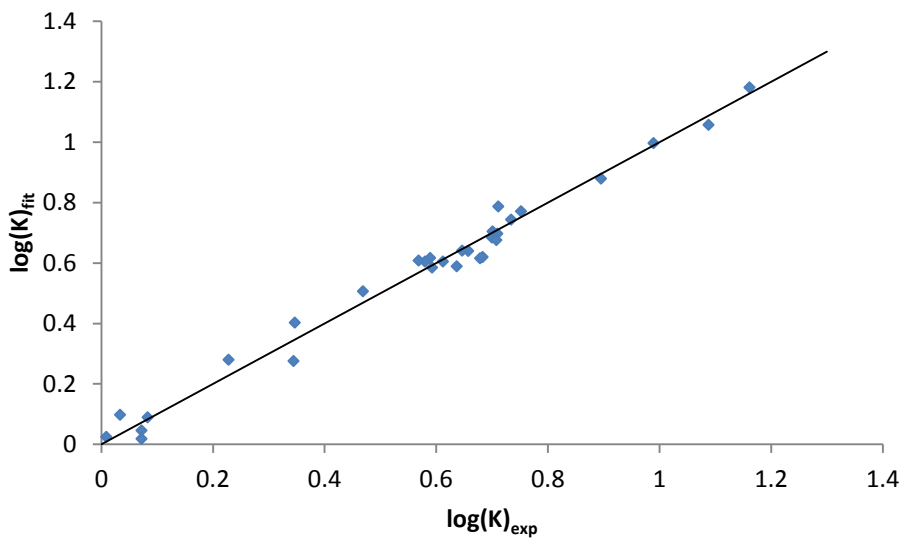


**Figure 4.5**  $\log(K)_{\text{fit}}$  as a function of  $\log(K)_{\text{exp}}$  for selected interaction parameters.

**Table 4.8** Calculated Solvent Descriptors using Selected Interaction Parameters

Solvent	Solvent Descriptors				
	s	a	b	v	c
(GVGVP) <sub>40</sub> + PBS	-0.363	0.219	-0.912	1.608	-0.099
(V <sub>3</sub> (VH) <sub>3</sub> ) <sub>4</sub> + PBS	-0.196	0.121	-0.715	1.189	0.000
(LQQ) <sub>12</sub> + PBS	-0.333	-0.150	-0.741	0.976	0.469
(GVGVP) <sub>40</sub>	0.106	-0.130	-0.767	1.056	0.000
(V <sub>3</sub> (VH) <sub>3</sub> ) <sub>4</sub>	0.506	-0.444	-0.344	0.343	-0.067

$$\log\left(K_{\text{co/sn}}^{(\text{GVGVP})_{40}+\text{PBS}}\right) = -0.363S + 0.219A - 0.912B + 1.608V - 0.099 \quad (4.11)$$

$$(N = 6; R^2 = 0.986; SE = 0.043; F = 90)$$

The coefficients in Eq. (4.11) are related to the difference in that specific interaction property between the coacervate and supernatant phases. Thus, for the (GVGVP)<sub>40</sub> + PBS system the coacervate phase is less dipolar/polarizable than the supernatant phase, indicated by a negative value for the s-coefficient. Also, the coacervate phase is a stronger hydrogen-bond base (positive a-coefficient), but a weaker hydrogen-bond acid (negative b-coefficient). The positive v-coefficient indicates the coacervate phase is able to interact with solutes by dispersive interactions and/or the energy required to create a cavity in the coacervate phase is less than that in the supernatant phase. Equations (4.12) through (4.15) represent the remaining solvent systems.

$$\log\left(K_{\text{co/sn}}^{(\text{V}_3(\text{VH})_3)_4+\text{PBS}}\right) = -0.196S + 0.121A - 0.715B + 1.189V + 0.000 \quad (4.12)$$

$$(N = 6; R^2 = 0.997; SE = 0.015; F = 450)$$

$$\log\left(K_{\text{co/sn}}^{(\text{LQQ})12+\text{PBS}}\right) = -0.333\text{S} - 0.150\text{A} - 0.741\text{B} + 0.976\text{V} + 0.469 \quad (4.13)$$

$$(\text{N} = 6; \text{R}^2 = 0.668; \text{SE} = 0.149; \text{F} = 4)$$

$$\log\left(K_{\text{co/sn}}^{(\text{GVGV})40}\right) = 0.106\text{S} - 0.130\text{A} - 0.767\text{B} + 1.056\text{V} + 0.000 \quad (4.14)$$

$$(\text{N} = 6; \text{R}^2 = 0.969; \text{SE} = 0.061; \text{F} = 41)$$

$$\log\left(K_{\text{co/sn}}^{(\text{V}_3(\text{VH})_3)_4}\right) = 0.506\text{S} - 0.444\text{A} - 0.344\text{B} + 0.343\text{V} - 0.067 \quad (4.15)$$

$$(\text{N} = 6; \text{R}^2 = 0.771; \text{SE} = 0.124; \text{F} = 5)$$

For most of the solutes investigated in this study the partition coefficient increased when the experiment was conducted in the presence of PBS (Table 4.4). In the solvent systems investigated the supernatant phase is predominantly water while the coacervate phase contains 40-50% protein by mass. Since the supernatant phase is predominantly water and likely to be more polar than the coacervate phase, it can be assumed that the dielectric constant of the supernatant phase is greater than that of the coacervate phase. [75] Therefore, during the partitioning process most of the PBS will partition into the supernatant phase. This increase in PBS within the supernatant phase results in an increase in the phase's cohesive energy density. Solvents of greater cohesive energy density require more energy to separate the solvent molecules and create a cavity of suitable size during solute transfer between phases. Using the data from the LFER analysis, the cavity formation descriptor (v-descriptor) is shown to decrease with

the addition of PBS (Table 4.8). This data is in agreement with the increase in cohesive energy density as a result of the addition of PBS and this increase in cavity formation energy causes lower solute partitioning into the supernatant phase.

For the two solutes investigated, vanillin and 4-nitrophenol, whose partition coefficient did not increase with the addition of PBS, their behavior can be explained from their pKa values. The pKa values for these solutes, 7.4 and 7.15 respectively, are close to the solute systems partitioning pH values. When these solutes partition in the systems without PBS a larger fraction remains in an uncharged state since the solution pH is below their pKa values. These materials in their uncharged state are more nonpolar and will prefer the coacervate phase over the more polar supernatant phase. When these solutes are introduced into the solvent systems with PBS a larger fraction of solute becomes ionized and therefore, becomes more soluble within the supernatant phase reducing the partition coefficient.

Combining the experimental data of measured partition coefficients with the LFER analysis shows that for greater compound encapsulation and potentially longer release rate the ELP tails, or ELP micelle core, should be preferably of greater hydrophobicity. While the critical transition temperature of  $(V_3(VH)_3)_4$  + PBS would indicate it is the most hydrophobic of all constructs examined, the solute partition coefficients in this system are lower than the  $(GVGVP)_{40}$  + PBS system, especially examining the most hydrophobic or least water soluble compound, ethyl paraben. This result would indicate that under physiological conditions (PBS pH 7.4) the coacervate produced from the  $(GVGVP)_{40}$  system is more hydrophobic than the  $(V_3(VH)_3)_4$  system and therefore, the same conclusion for the micelle interior. If a relationship exists

between the ELP transition temperature, hydrophobicity, and solute partitioning, it would be difficult to design an ELP structure that provides high encapsulation within the micelle interior based only on using transition temperature as a measure of hydrophobicity.

According to the LFER analysis, the dominate interaction under physiological conditions is the dispersive energy and cavity formation term. Dispersive interactions are dominate in non-polar hydrocarbon chains and influence solute retention time on reverse phase C<sub>18</sub> HPLC columns.

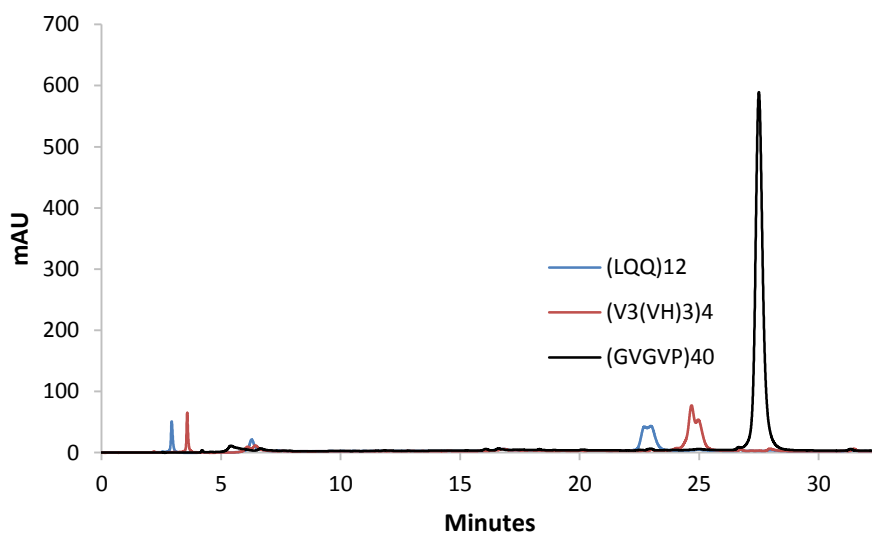


**Figure 4.6** Chromatogram showing (LQQ)<sub>12</sub>, (V<sub>3</sub>(VH)<sub>3</sub>)<sub>4</sub>, and (GVGVP)<sub>40</sub> ELP. Mobile phase A composition was 5% (v/v) acetonitrile in PBS. Mobile phase B composition was 100% acetonitrile. Gradient elution 0 to 50% B over 30 minutes.

According to HPLC retention time on a C<sub>18</sub> stationary phase column using PBS (0.15 M NaCl, 0.01 M Na<sub>3</sub>PO<sub>4</sub>, pH 7.4) as the mobile phase, the gradient elution pattern suggests the (GVGVP)<sub>40</sub> construct is of greater dispersive interaction energy than the

(V<sub>3</sub>(VH)<sub>3</sub>)<sub>4</sub> construct, which is in agreement with the partitioning and LFER data (Figure 4.6). Therefore, during the design of future ELP constructs for their use in drug encapsulation and delivery, it is suggested to use ELP transition temperatures as only an approximation of hydrophobicity, and this data should be combined with HPLC relative retention times to measure ELP dispersive interaction energy as a better indicator of solute partitioning behavior.

#### *Doxorubicin Partitioning and LFER Analysis*

Doxorubicin is an anthracycline chemotherapeutic commonly used to treat many different forms of cancer (Figure 4.7). Unfortunately, the clinical use of anthracyclines is limited by dose related cardiomyopathy and becomes more prevalent during treatment due to the cumulative effect of the drug. [76] Since myocardial injury is known to occur cumulatively, starting from the first dose of treatment, there has been much effort in the development a drug delivery system or formulation that reduces this damaging side effect. [76, 77, 78] In an attempt to decrease its cumulative cardiotoxicity and increase its therapeutic efficiency, several authors have investigated doxorubicin's ability to be encapsulated or conjugated within micelles and liposomes. [76, 79, 80, 81, 82, 83]



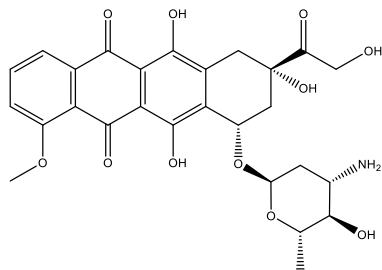


**Figure 4.7** Molecular structure of doxorubicin

Supplied as its hydrochloride salt, doxorubicin has good water solubility (29 mg/mL) and with a high molar absorption coefficient it is easy to detect by UV-VIS spectroscopy at low concentrations. To investigate the potential of an ELP drug delivery platform to encapsulate doxorubicin this solute was partitioned, under physiological conditions, in the most hydrophobic solvent system investigated in this study, (GVGVP)<sub>40</sub> + PBS.

Abraham descriptors for doxorubicin were obtained from the Open Abraham Descriptor Data Explorer (Table 4.9). [84] The measured partition coefficient and 95% confidence interval for doxorubicin was 150 and 44 respectively (Figure 4.8).

**Table 4.9** Solute Descriptors for Doxorubicin Obtained from Open Abraham Descriptor Database

Solute	Solute Descriptors				
	E	S	A	B	V
5-Fluorouracil	0.72	0.84	0.57	1.02	0.7693
Acetaminophen	1.06	1.63	1.04	0.86	1.1724
Vanillin	0.99	1.30	0.31	0.68	1.1313
Phenol	0.805	0.89	0.6	0.3	0.7751
4-Nitrophenol	1.07	1.72	0.82	0.26	0.9493
Ethyl Paraben	0.91	1.44	0.73	0.45	1.2722
Doxorubicin	3.63	4.1	1.3	3.41	3.728

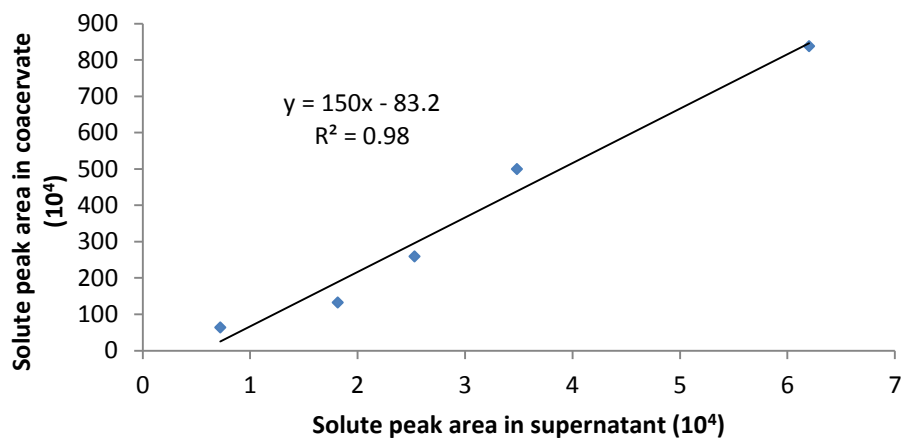


**Figure 4.8** Partitioning data for doxorubicin in the (GVGVP)<sub>40</sub> + PBS solvent system.

**Table 4.10** Solvent Descriptors for Solvent System (GVGVP)<sub>40</sub> + PBS Obtained from Linear Regression of Solute Set with and without Including Doxorubicin

Solvent	Solvent Descriptors					
	e	s	a	b	v	c
(GVGVP) <sub>40</sub> + PBS	0.471	-0.572	0.276	-0.919	1.646	-0.336
(GVGVP) <sub>40</sub> + PBS with Dox.	0.363	-0.526	0.264	-0.921	1.632	-0.273

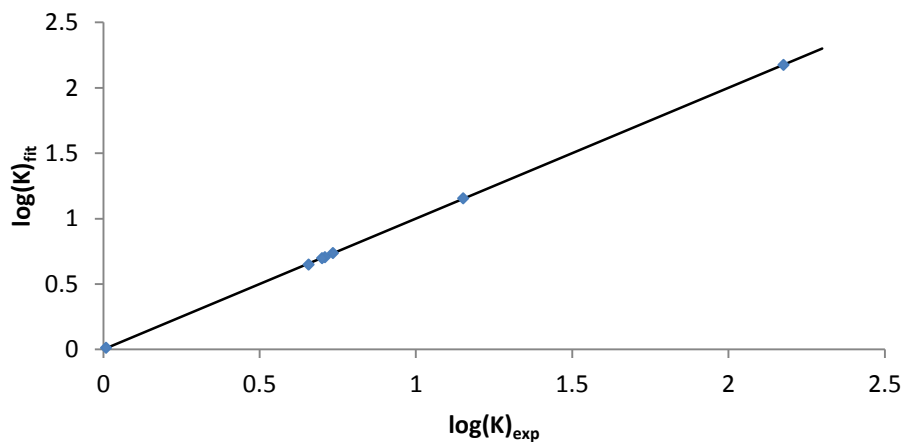


**Figure 4.9**  $\log(K)_{\text{fit}}$  as a function of  $\log(K)_{\text{exp}}$  for the (GVGVP)<sub>40</sub> + PBS solvent system with doxorubicin included in the solute set.

With the addition of doxorubicin to the solute set, the larger number of solutes allows the inclusion of the ‘eE’ interaction descriptor while still providing an over-determined condition during regression analysis (Table 4.10, Figure 4.9). As shown in Table 4.10 the inclusion of doxorubicin into the solute set has changed the solvent descriptors. Using the original solvent descriptors, where the solute system did not include doxorubicin to calculate the partition coefficient of doxorubicin, resulted in an overestimation of its partition coefficient, but as expected all other solutes fit the model perfectly (Table 4.11). A possible explanation for this result is the large difference in the solute descriptors for doxorubicin compared to all other solutes investigated (Table 4.9). When the partition coefficients were calculated using the LFER model that includes doxorubicin in the solute set, Eq. (4.16), it is shown that this model can accurately predicts the partition coefficient of doxorubicin. Also, this model shows reasonable agreement between the calculated fit and experimental partition coefficients for all remaining solutes within the set (Table 4.11).

**Table 4.11** Calculated Solute Partition Coefficients using Solvent Descriptors from Table 4.10 and Solute Descriptors from Table 4.9

Solute	$K_{exp}$	$K_{fit}$	
		With doxorubicin.	Without doxorubicin
5-Fluorouracil	1.02	1.03	1.02
Acetaminophen	4.54	4.47	4.54
Vanillin	5.12	5.07	5.12
Phenol	5.01	4.99	5.01
4-Nitrophenol	5.42	5.46	5.42
Ethyl Paraben	14.2	14.3	14.2
Doxorubicin	150	150	245

$$\log\left(K_{\text{co/sn}}^{(\text{GVGVP})40+\text{PBS}}\right) = 0.363E - 0.526S + 0.264A - 0.921B + 1.632V - 0.273 \quad (4.16)$$

$$(N = 7; R^2 = 1.00; SE = 0.086; F = 4,707)$$

## CHAPTER V

### CONCLUSION

To provide insight into the potential use of elastin-like polypeptides as a drug delivery platform solute partitioning was performed using three ELP constructs with varying hydrophobicity. Protein solutions were prepared with and without the addition of PBS to investigate the influence of PBS on solute partitioning. All partitioning data was subject to a LFER analysis to characterize the two phases that resulted from the partitioning process. Due to the clinical importance of doxorubicin, it was partitioned into the most hydrophobic system investigated, (GVGVP)<sub>40</sub> + PBS, in an effort to maximize its encapsulation efficiency. Finally, doxorubicin was added to the solvent set and the LFER coefficients for the (GVGVP)<sub>40</sub> + PBS solvent system were recalculated.

The LFER results indicate of all 5 interaction descriptors the two most dominate were the dispersive interaction and cavity formation term followed by the solvents hydrogen bond acidity. For the solutes investigated, greater partitioning into the coacervate phase was observed in ELP systems that were determined to have a stronger dependence on dispersive interactions and solute size. After the addition of doxorubicin

to the solute set and recalculation of the (GVGVP)<sub>40</sub> + PBS solvent system's LFER coefficients, reasonable agreement between the calculated fit and experimental partition coefficients was observed.

## BIBLIOGRAPHY

1. Shewry, P. R.; Tatham, A. S.; Baliley, A. *Elastomeric Proteins: Structures, Biomechanical Properties, and Biological Roles*; Cambridge University Press: New York, 2002.
2. Urry, D. W. Physical Chemistry of Biological Free Energy Transduction As Demonstrated by Elastic Protein-Based Polymers. *Journal of Physical Chemistry B* **1997**, *101* (51), 11007-11028.
3. Meyer, D. E.; Chilkoti, A. Genetically Encoded Synthesis of Protein-Based Polymers with Precisely Specified Molecular Weight and Sequence by Recursive Directional Ligation: Examples from the Elastin-like Polypeptide System. *Biomacromolecules* **2002**, *3* (2), 357-367.
4. McDaniel, J.; Machay, J.; Chilkoti, A. Recursive Directional Ligation by Plasmid Reconstruction Allows Rapid and Seamless Cloning of Oligomer Genes. *Biomacromolecules* **2010**, *11* (4), 944.
5. Amiram, M.; Quiroz, F.; Callahan, D.; Chilkoti, A. Highly Parallel Method for Synthesis of DNA Repeats Enables Discovery of "Smart" Protein Polymers. *Nature Materials* **2011**, *10* (2), 141.
6. Ghoorchian, A.; Cole, J. T.; Holland, N. B. Thermoreversible Micelle Formation Using a Three-Armed Star Elastin-like Polypeptide. *Macromolecules* **2010**, *43*, 4340-4345.

7. Cho, Y.; Zhang, Y.; Christensen, T.; Sagle, L. B.; Chilkoti, A.; Cremer, P. S. Effect of Hofmeister Anions on the Phase Transition Temperature of Elastin-like Polypeptides. *Journal of Physical Chemistry B* **2008**, *112*, 13765-13771.
8. Rembert, K. B.; Paterova, J.; Hilty, C.; Jungwirth, P.; Cremer, P. S. Molecular Mechanisms of Ion-Specific Effects on Proteins. *Journal of the American Chemical Society* **2012**, *134*, 10039-10046.
9. Meyer, D. E.; Chilkoti, A. Quantification of the Effects of Chain Length and Concentration on the Thermal Behavior of Elastin-like Polypeptides. *Biomacromolecules* **2004**, *5*, 846-851.
10. Ghoorchian, A.; Holland, N. B. Molecular Architecture Influences the Thermally Induced Aggregation Behavior of Elastin-like Polypeptides. *Biomacromolecules* **2011**, *12*, 4022-4029.
11. Dreher, M. R.; Raucher, D.; Balu, N.; Colvin, M.; Ludeman, S.; Chilkoti, A. Evaluation of an elastin-like polypeptide-doxorubicin conjugate for cancer therapy. *Journal of Controlled Release* **2003**, *91*, 31-43.
12. MacKay, J. A.; Callahan, D. J.; FitzGerald, K. N.; Chilkoti, A. Quantitative Model of the Phase Behavior of Recombinant pH-Responsive Elastin-like Polypeptides. *Biomacromolecules* **2010**, *11*, 2873-2879.



13. Tang, M. Synthesis and Characterization of pH Responsive Elastin-like Polypeptides with Different Configurations. MS Thesis, Cleveland State University, Cleveland, OH, 2013.
14. Martin, R.; Helm, E.; Holland, N. B. Characterizing Stimuli-Responsive Materials for Drug Delivery: Interactions with Model Compounds and pH Responsive Behavior. *Cleveland State University Student Poster Session*, Cleveland, OH, 2015.
15. Urry, D. W. *What Sustains Life? Consilient Mechanisms for Protein-Based Machines and Materials*; Birkhauser Boston: Boston, 2006.
16. Maeda, H.; Seymour, L. W.; Miyamoto, Y. Conjugates of Anticancer Agents and Polymers: Advantages of Macromolecular Therapeutics in vivo. *Bioconjugate Chemistry* **1992**, *3*, 351-362.
17. Raucher, D.; Chilkoti, A. Enhanced Uptake of a Thermally Responsive Polypeptide by Tumor Cells in Response to its Hyperthermia-mediated Phase Transition. *Cancer Research* **2001**, *61*, 7163-7170.
18. Meyer, D. E.; Kong, G. A.; Dewhirst, M. W.; Zalutsky, M. R.; Chilkoti, A. Targeting a Genetically Engineered Elastin-like Polypeptide to Solid Tumors by Local Hyperthermia. *Cancer Research* **2001**, *61* (4), 1548-1554.

19. Moktan, S.; Ryppa, C.; Kratz, F.; Raucher, D. A thermally responsive biopolymer conjugated to an acid-sensitive derivative of paclitaxel stabilizes microtubules, arrests cell cycle, and induces apoptosis. *Investigational New Drugs* **2012**, *30*, 236-248.
20. Wright, E. R.; Conticello, V. P. Self-assembly of block copolymers derived from elastin-mimetic polypeptide sequences. *Advanced Drug Delivery Reviews* **2003**, *54*, 1057-1073.
21. Kim, W.; Xiao, J.; Chaiknof, E. L. Recombinant Amphiphilic Protein Micelles for Drug Delivery. *Langmuir* **2011**, *27* (23), 14329-14334.
22. Adams, S.; Shamji, M.; Nettles, D.; Hwang, P.; Setton, L. Sustained Release of Antibiotics from Injectable and Thermally Responsive Polypeptide Depots. *Journal of Biomedical Materials Research Part B: Applied Biomaterials* **2009**, *90* (1), 67-74.
23. Ghoorchian, A.; Vandemark, K.; Freeman, K.; Kambow, S.; Holland, N. B.; Streletzky, K. A. Size and Shape Characterization of Thermoreversible Micelles of Three-Armed Star Elastin-like Polypeptides. *The Journal of Physical Chemistry B* **2013**, *117*, 8865-8874.
24. Smith, J.; Van Ness, H.; Abbott, M. *Introduction to Chemical Engineering Thermodynamics*; McGraw-Hill: New York, 2005.

25. Zaslavsky, B. Y. *Aqueous Two-Phase Partitioning: physical chemistry and bioanalytical applications*; Marcel Dekker: New York, 1995.
26. Sophianopoulos, A.; Van Holde, K. Evidence for Dimerization of Lysozyme in Alkaline Solution. *The Journal of Biological Chemistry* **1961**, 236 (12), PC82-PC83.
27. Gulyaeva, N.; Zaslavsky, A.; Lechner, P.; Chlenov, M. M. O.; Chait, A.; Kipnis, V.; Zaslavsky, B. Relative hydrophobicity and lipophilicity of drugs measured by aqueous two-phase partitioning, octanol-buffer partitioning and HPLC. A simple model for predicting blood-brain distribution. *European Journal of Medicinal Chemistry* **2003**, 38, 391-396.
28. Abraham, M.; Ibrahim, A.; Acree, W. Air to liver partition coefficients for volatile organic compounds and blood to liver partition coefficients for volatile organic compounds and drugs. *European Journal of Medicinal Chemistry* **2007**, 42 (6), 743-751.
29. Gulyaeva, N.; Zaslavsky, A.; Lechner, P.; Chait, A.; Zaslavsky, B. Relative hydrophobicity of organic compounds measured by partitioning in aqueous two-phase systems. *Journal of Chromatography B* **2000**, 743, 187-194.
30. Archivio, A.; Ruggieri, F.; Mazzeo, P.; Tettamanti, E. Modelling of retention of pesticides in reverse phase high performance liquid chromatography. *Analytica Chimica Acta* **2007**, 593, 140-151.

31. Abraham, M.; Whiting, G.; Doherty, R.; Shuely, W. Hydrogen Bonding. Part 13. A new method for the characterization of glc stationary phases. *Journal of the Chemical Society Perkin Transactions 2* **1990**, 1990 (8), 1451-1460.
32. Zhao, Q.; Yang, K.; Li, W.; Xing, B. Concentration-dependent polyparameter linear free energy relationships to predict organic compound sorption on carbon nanotubes. *Scientific Reports* **2014**, 4 (3888), 1-7.
33. Abraham, M. J.; Smith, R. E. Prediction of solubility of drugs and other compounds in organic solvents. *Journal of Pharmaceutical Science* **2010**, 99 (3), 1500-1515.
34. Sprunger, L. M.; Achi, S. S.; Racheal, P.; Acree, W.; Abraham, M. Development of Abraham model correlations for solvation characteristics of secondary and branched alcohols. *Fluid Phase Equilibria* **2010**, 288, 121-127.
35. Abraham, M.; Chadha, H.; Whiting, G.; Mitchell, R. Hydrogen Bonding. 32. An Analysis of Water-Octanol and Water-Alkane Partitioning and the log P Parameter of Seiler. *Journal of Pharmaceutical Sciences* **1994**, 83 (8), 1085-1100.
36. Acree, W.; Abraham, M. Solubility of Crystalline Nonelectrolyte Solutes in Organic Solvents. *Journal of Solution Chemistry* **2002**, 31 (4), 293-303.

37. Pagliara, A.; Caron, G.; Lisa, G.; Fan, W.; Gaillard, P.; Carrupt, P.; Testa, B.; Abraham, M. Solvatochromic analysis of di-n-butyl ether/water partition coefficients as compared to other solvent systems. *Journal of the Chemical Society Perkin Transactions 2* **1997**, 1997 (12), 2639-2643.
38. Abraham, M. H.; Acree, W. J. Characterization of the water-isopropyl myristate system. *International Journal of Pharmaceutics* **2005**, 294, 121-128.
39. Abraham, M.; Ibrahim, A.; Zissimos, A. Determination of sets of solute descriptors from chromatographic measurements. *Journal of Chromatography A* **2004**, 1037 (1-2), 29-47.
40. Abraham, M. H.; McGowan, J. C. The Use of Characteristic Volumes to Measure Cavity Terms in Reversed Phase Liquid Chromatography. *Chromatographia* **1987**, 23 (4), 243-246.
41. Zissimos, A. M.; Abraham, M. H.; Barker, M. C.; Box, K. J.; Tam, K. Y. Calculation of Abraham descriptors from solvent-water partition coefficients in four different systems; evaluation of different methods of calculation. *Journal Chemical Society Perkin Transactions 2* **2002**, 470-477.
42. Cacelli, I.; Campanile, S.; Giolitti, A.; Molin, D. Theoretical Prediction of the Abraham Hydrogen Bond Acidity and Basicity Factors. *Journal of Chemical Information and Modeling* **2005**, 45 (2), 327-333.

43. Lamarche, O.; Platts, J.; Hersey, A. Theoretical predictions of the polarity/polarizability parameter. *Physical Chemistry Chemical Physics* **2001**, *3*, 2747-2753.
44. Bradley, J.-C.; Abraham, M.; Acree, W.; Lang, A. Determination of Abraham model solute descriptors for the monomeric and dimeric forms of trans-cinnamic acid using measured solubilities from the Open Notebook Science Challenge. *Chemistry Central Journal* **2015**, *9* (1), 1-6.
45. Wilson, A.; Tian, A.; Chou, V. Experimental and predicted solubilities of 3,4-dichlorobenzoic acid in select organic solvents and in binary aqueous-ethanol mixtures. *Physics and Chemistry of Liquids* **2012**, *50* (3), 324-335.
46. Abraham, M.; Acree, W.; Earp, C. Studies on the hydrogen bond acidity, and other descriptors and properties for hydroxyflavones and hydroxyisoflavones. *Journal of Molecular Liquids* **2015**, *208*, 363-372.
47. Ettre, L.; Sakodinskii, K. M. S. Tswett and the Discovery of Chromatography I: Early Work (1899-1903). *Chromatographia* **1993**, *35* (3), 223.
48. Ettre, L.; Sakodinskii, K. M. S. Tswett and the Discovery of Chromatography II: Completion of the Development of Chromatography (1903-1910). *Chromatographia* **1993**, *35* (5), 329.

49. Fekete, S.; Olah, E.; Fekete, J. Fast liquid chromatography: The domination of core-shell and very fine particles. *Journal of Chromatography A* **2012**, *1228*, 71.
50. Robards, K.; Haddad, P. R.; Jackson, P. *Principles and Practice of Modern Chromatographic Methods*; Academic Press Inc: San Diego, 1994.
51. Poppe, H. Some reflections on speed and efficiency of modern chromatographic methods. *Journal of Chromatography A* **1997**, *778*, 3-21.
52. Villiers, A. d.; Lestremau, F.; Szucs, R.; Gelebart, S.; David, F.; Sandra, P. Evaluation of ultra performace liquid chromatography Part I. Possibilities and limitations. *Journal of Chromatography A* **2006**, *1127*, 60-69.
53. Guillarme, D.; Nguyen, D. T.; Rudaz, S.; Veuthey, J.-L. Recent developments in liquid chromatography - impact on qualitative and quantitative performance. *Journal of Chromatography A* **2007**, *1149*, 20-29.
54. Fanali, S.; Rocchi, S.; Chankvetadze, B. Use of novel phenyl-hexyl core-shell particles in nano-LC. *Electrophoresis* **2013**, *34*, 1737-1742.
55. Fekete, S.; Veuthey, J.-L.; Guillarme, D. Comparison of the most recent chromatographic approaches applied for fast and high resolution separations: Theory and practice. *Journal of Chromatography A* **2015**, *1408*, 1-14.

56. Fontana, A.; Antonioli, A.; Bottini, R. Development of a high pressure liquid chromatography method based on a core-shell column approach for the rapid determination of multiclass polyphenols in grape pomaces. *Food Chemistry* **2016**, *192*, 1-8.
57. Halasz, I.; Endeke, R.; Asshauer, J. Ultimate limits in high pressure liquid chromatography. *Journal of Chromatography A* **1975**, *112*, 37-80.
58. Martin, M.; Eon, C.; Guiochon, G. Study of the pertinency of pressure in liquid chromatography: 1. theoretical analysis. *Journal of Chromatography A* **1974**, *99*, 357-376.
59. Li, X.; Woodman, M.; Wang, S. C. High-performance liquid chromatography with fluorescence detection for the rapid analysis of pheophytins and pyropheophytins in virgin olive oil. *Journal of Separation Science* **2015**, *38*, 2813-2818.
60. Kahsay, G.; van Schepdael, A.; Hoogmartens, J. Analysis of Temocillin and Impurities by Reverse Phase Liquid Chromatography: Development and Validation of the Method. *Chromatographia* **2014**, *77*, 1323-1331.
61. Badea, I.; Ciutaru, D.; Lazar, L.; Nicolescu, D.; Tudose, A. Rapid HPLC method for the determination of paclitaxel in pharmaceutical forms without separation. *Journal of Pharmaceutical and Biomedical Analysis* **2004**, *34*, 501-507.



62. Kahsay, G.; Shraim, F.; Villatte, P.; Rotger, J.; Cassus-Coussere, C.; Van Schepdael, A.; Hoogmartens, J.; Adams, E. Development and validation of a reverse phase liquid chromatographic method for analysis of oxytetracycline and related impurities. *Journal of Pharmaceutical and Biomedical Analysis* **2013**, *75*, 199-206.
63. Rheodyne - Manual Dual Mode Sample Injectors for HPLC.  
<http://kinesis.co.uk/knowledgebase/rheodyne-dual-mode-sample-injectors/>  
(accessed Sept. 1, 2015).
64. Li, J.; Bi, Y.; Lie, W.; Sun, S. Simultaneous Analysis of Tertiary Butylhydroquinone and 2-tert-Butyl-1,4-benzoquinone in Edible Oils by Normal-Phase High-Performance Liquid Chromatography. *Journal of Agricultural and Food Chemistry* **2015**, *63*, 8584-8591.
65. Gomez-Caravacaa, A.; Verardoc, V.; Berardinelli, A.; Marconi, E.; Caboni, M. A chemometric approach to determine the phenolic compounds in different barley samples by two different stationary phases: A comparison between C18 and pentafluorophenyl core shell columns. *Journal of Chromatography A* **2014**, *1355*, 134-142.
66. Lesellier, E.; West, C. Description and comparison of chromatographic tests and chemometric methods for packed column classification. *Journal of Chromatography A* **2007**, *1158*, 329-360.

67. Klejdus, B.; Vacek, J.; Lojkova, L.; Benesova, L.; Kuban, V. Ultrahigh-pressure liquid chromatography of isoflavones and phenolic acids on different stationary phases. *Journal of Chromatography A* **2008**, *1195*, 52-59.
68. nanoComposix. Characterization Techniques.  
<http://nanocomposix.com/pages/characterization-techniques> (accessed Sept. 1, 2015).
69. Kracke, B.; Cole, J. T.; Kaiser, C. J.; Hellenkamp, B. Thermoswitchable Nanoparticles Based on Elastin-like Polypeptides. *Macromolecules* **2015**, *48*, 5868.
70. Cole, J. T.; Holland, N. B. Multifunctional nanoparticles for use in theranostic applications. *Drug Delivery and Translational Research* **2015**, *5*, 295.
71. Golemis, E. Protein Purification by Inverse Transition Cycling. In *Protein-protein interactions: a molecular cloning manual*; Cold Spring Harbor Laboratory Press: Cold Spring Harbor, 2001; pp 329-343.
72. Clarke, E. D.; Mallon, L. J. The Determination of Abraham Descriptors and Their Application to Crop Protection Research. In *Modern Methods in Crop Protection Research*; Wiley-VCH, 2013; pp 273-305.

73. Zissimos, A. M.; Abraham, M. H.; Du, C. M.; Valko, K.; Bevan, C.; Reynolds, D.; Wood, J.; Tam, K. Y. Calculation of Abraham descriptors from experimental data from seven HPLC systems; evaluation of five different methods of calculation. *Journal of the Chemical Society Perkin Transactions 2* **2002**, 2001-2010.
74. Abraham, M. H.; Abraham, R. J.; Acree, W. E.; Aliev, A. E.; Leo, A. J.; Whaley, W. L. An NMR Method for the Quantitative Assessment of Intermolecular Hydrogen Bonding; Application to Physicochemical, Environmental, and Biochemical Properties. *The Journal of Organic Chemistry* **2014**, 79, 11075-11083.
75. Israelachvili, J. N. *Intermolecular and Surface Forces Third Edition*; Academic Press: Waltham, 2011.
76. Harris, L.; Batist, G.; Belt, R.; Rovira, D.; Navari, R.; Azarnia, N.; Welles, L.; Winer, E. Liposome-Encapsulated Doxorubicin Compared with Conventional Doxorubicin in a Randomized Multicenter Trial as First-Line Therapy of Metastatic Breast Carcinoma. *Cancer* **2002**, 94 (1), 25-36.
77. M, B.; Mason, J.; Bristow, M.; Daniels, J. Anthracycline cardiomyopathy monitored by morphologic changes. *Cancer Treatment Reports* **1978**, 62, 865-872.

78. Hale, J.; Lewis, I. Anthracyclines: cardiotoxicity and its prevention. *Archives of Disease in Childhood* **1994**, *71*, 457-462.
79. Sang Yoo, H.; Gwan Park, T. Biodegradable polymeric micelles composed of doxorubicin conjugated PLGA-PEG block copolymer. *Journal of Controlled Release* **2001**, *70*, 63-70.
80. Batist, G.; Ramakrishnan, G.; Rao, C.; A, C.; Gutheil, J.; Guthrie, T.; Shah, P.; Khojasteh, A.; Nair, M.; Hoelzer, K. Reduced Cardiotoxicity and Preserved Antitumor Efficacy of Liposome-Encapsulated Doxorubicin and Cyclophosphamide Compared With Conventional Doxorubicin and Cyclophosphamide in a Randomized, Multicenter Trial of Metastatic Breast Cancer. *Journal of Clinical Oncology* **2001**, *18* (5), 1444-1454.
81. Cuong, N.-V.; Jiang, J.-L.; Li, Y.-L.; Chen, J.-R.; Jwo, S.-C.; Hsieh, M.-F. Doxorubicin-Loaded PEG-PCL-PEG Micelle Using Xenograft Model of Nude Mice: Effect of Multiple Administration of Micelle on the Suppression of Human Breast Cancer. *Cancers* **2011**, *3*, 61-78.
82. Kim, D.; Gao, Z. G.; Lee, E. S.; Bae, Y. H. In Vivo Evaluation of Doxorubicin-Loaded Polymeric Micelles Targeting Folate Receptors and Early Endosomal pH in Drug-Resistant Ovarian Cancer. *Molecular Pharmaceutics* **2009**, *6* (5), 1353-1362.

83. Dube, N.; Shu, J.; Dong, H.; Seo, J.; Ingham, E. Evaluation of Doxorubicin-Loaded 3-Helix Micelles as Nanocarriers. *Biomacromolecules* **2013**, *14* (10), 3697-3705.
84. Acree Jr, W.; Bradley, J.-C.; Lang, A. Open Abraham Descriptor Data Explorer. <http://lxsrv7.oru.edu/~alang/abrahamdescriptors/> (accessed Sept. 1, 2015).
85. Souza, S. D. A Review of In Vitro Drug Release Test Methods for Nano-Sized Dosage Forms. *Advances in Pharmaceutics* **2014**, *2014*, 1-12.
86. Modi, S.; Anderson, B. D. Determination of Drug Release Kinetics from Nanoparticles: Overcoming Pitfalls of the Dynamic Dialysis Method. *Molecular Pharmaceutics* **2013**, *10* (8), 3076-3089.

## **APPENDIX**

### **Appendix A**

#### **Lysogeny Broth (LB) Media Preparation**

1. To prevent boil-over during autoclaving the media vessel should only be filled to a maximum of 75% volume. The appropriate media vessel was charged with 5 g/L media yeast extract, 10 g/L media peptone, 5 g/L media sodium chloride then filled to the final volume using deionized water.
2. Media sterilization was performed using a steam autoclave (Cycle: 121°C for 45 min).
3. Once media was cooled to room temperature ampicillin was added at a concentration of 100 mg/L media.

#### **Protein Expression**

##### **One Liter Expression Scale**

1. For each liter of expression media, starter cultures were grown from a frozen glycerol bacterial stock culture by inoculating two 15 mL sterile culture tubes filled with 10 mL of previously prepared LB media with ampicillin.
2. The inoculated media was grown at 37°C overnight (approximately 16 hours) on a shaker table (250 rpm).

3. The following day both starter cultures were added to a 2 L Erlenmeyer flask charged with 1 L LB media with ampicillin at 37°C.
4. This culture was grown at 37°C on a shaker table (250 rpm) while monitoring the growth rate using a UV-VIS spectrometer.
5. Growth was allowed to continue until the optical density measured at 600 nm (OD<sub>600</sub>) was between 0.8 and 1.2 absorbance units (4-8 hours).
6. Once the optical density reached the target range the culture was induced using 200-240 mg/L media isopropyl β-D-1-thiogalactopyranoside (IPTG).
7. Induction was allowed to proceed for a minimum of 5 hours then bacteria were isolated by centrifugation (20°C, 10,000xg, 10 min).
8. When necessary the isolated pellet was stored overnight at -20°C.

### Six Liter Expression Scale

1. Starter cultures were grown from a frozen glycerol bacterial stock culture by inoculating two 15 mL sterile culture tubes filled with 10 mL of previously prepared LB media with ampicillin.
2. The starter cultures were grown for 4 hours at 37°C on a shaker table (250 rpm) then transferred to a 2 L Erlenmeyer flask containing 1 liter of previously prepared LB media with ampicillin.
3. This 1 liter starter culture was grown overnight (approximately 16 hours) at 25°C on a shaker table (200 rpm).

4. The following day, the bacteria from the 1 liter starter culture was isolated by centrifugation (20°C, 10,000xg, 10 min) and re-suspended by gently swirling in 250 mLs sterilized deionized water or previously prepared LB media.
5. Once re-suspended the pellet suspension was transferred to the final expression vessel.

The final expression vessel consisted of an 8 liter wide mouth polypropylene mason jar (Bel-Art #109170000) filled to 6 liters LB media with ampicillin. This media was prepared and steam autoclaved (Cycle: 121°C for 90 min) in the expression vessel the previous day then allowed to equilibrate to 37°C overnight in a temperature controlled water bath.

6. Using a steam autoclaved air stone (autoclaved with the final expression vessel and media) media oxygenation and agitation was performed by bubbling sterile filtered air into the media at a rate of approximately 1 liter per hour. Occasionally it was necessary to reduce the air flow rate due to excessive foaming of the media.  
Note: While this combined agitation and oxygenation method was successful, reducing the air flow rate to prevent excess foaming resulted in increasing the time necessary to reach the required OD<sub>600</sub> range. If this increase in time to reach the required OD<sub>600</sub> range is due to the reduced agitation at the lower air flow rate then a better method would be to separate the agitation and oxygenation techniques. By stirring the media using an external stirring source while providing oxygenation at an air flow rate that prevents excessive media foaming growth rate may be increased reducing the time to reach the required OD<sub>600</sub> range.



7. After inoculation of the 6 L culture, growth was monitored by UV-VIS spectroscopy.
8. Once an OD<sub>600</sub> of 0.8 to 1.2 was obtained (4-8 hours) the culture was induced using IPTG (200-240 mg/L media).
9. Induction was allowed to proceed for a minimum of 5 hours then bacteria were isolated by centrifugation (20°C, 10,000xg, 10 min).
10. When necessary the isolated pellet was stored overnight at -20°C.

## **Appendix B**

### **Protein Extraction Protocol**

1. For both the 1 liter and 6 liter expression volumes protein extraction from the bacterial pellet was performed by lysing the bacterial cells followed by cold centrifugation. Cell lysis was performed by combining all bacterial pellets into 30 mL cold (5-10°C) deionized water per liter of expression culture.
2. Next, pulse sonication (550 Sonic Dismembrator, Fisher Scientific) was performed to disrupt the bacterial wall and allow protein to be extracted. For the 1 L expression volume, sonication time was 5 minutes and at the 6 L expression scale the sonication time was doubled to 10 minutes. Sonication pulse sequences were identical at both volumes (<10°C, pulse cycle: 10 s on 20 s off, 100% power).
3. After sonication, the cell lysate (Cell Lysate Solution) was cooled in an ice-bath below 5°C then cold centrifuged (3°C, 20,000xg, 20 min) to remove insoluble cellular material.
4. Finally, the aqueous protein solution (Crude Protein Solution) was decanted from the insoluble material for further purification by inverse transition cycling.

### **Protein Purification by Inverse Temperature Cycling**

Protein purification was performed by inverse transition cycling (ITC). Three rounds of ITC were performed using deionized water for all pellet re-suspensions. Re-

suspension volumes for each round of purification were 15, 5, and 1 mL/L culture respectively. Pellet re-suspensions were performed using pulse sonication (<10°C, pulse cycle: 10 s on 20 s off, 100% power) when necessary.

### Inverse Transition Cycling Protocol for Construct (GVGVP)<sub>40</sub>

1. For construct (GVGVP)<sub>40</sub>, the ITC protocol began by quickly heating the crude protein solution obtained after cold centrifugation to 55°C using a 70°C hot water bath.
2. Once heated to temperature the protein solution was allowed to sit in an incubator for 30 minutes at 55°C. During this time the ELP and additional impurities separated from solution.
3. After this incubation period, the aggregated ELP and supernatant phases were separated by hot centrifugation (40°C, 20,000xg, 10 min) followed by decanting of the supernatant phase.
4. Next, the pellet containing ELP was re-suspended in 15 mL/L culture deionized water with cooling and slight mixing.
5. Once re-suspended, the protein solution was centrifuged cold (3°C, 20,000xg, 10 min) to remove insoluble impurities.
6. This completes one round of ITC, two additional rounds were performed using re-suspension volumes of 5 and 1 mL/L culture respectively.
7. After all rounds of ITC were complete the protein solution was filtered through a 0.22 µm syringe filter and stored at 4°C or lyophilized until needed.

## Inverse Transition Cycling Protocol for Construct (LQQ)<sub>12</sub>

The ITC protocol for construct (LQQ)<sub>12</sub> was identical to that of (GVGV)<sub>40</sub> with the exception that sodium chloride was added to all hot cycles (2 M NaCl final concentration). Pellet re-suspensions were performed using pulse sonication (<10°C, pulse cycle: 10 s on 20 s off, 100% power) when necessary.

1. For construct (LQQ)<sub>12</sub>, the ITC protocol began by adding solid sodium chloride to the crude protein solution obtained after cold centrifugation to a final concentration of 2 M NaCl.
2. Next, this solution was quickly heated to 55°C using a 70°C hot water bath.
3. Once heated to temperature the protein solution was allowed to sit in an incubator for 30 minutes at 55°C. During this time the ELP and additional impurities separated from solution.
4. After this incubation period, the aggregated ELP and supernatant phases were separated by hot centrifugation (40°C, 20,000xg, 10 min) followed by decanting of the supernatant phase.
5. Next, the ELP phase was re-suspended in 15 mL/L culture deionized water with cooling and slight mixing.
6. Once re-suspended, the protein solution was centrifuged cold (3°C, 20,000xg, 10 min) to remove insoluble impurities.
7. This completes one round of ITC, two additional rounds were performed using re-suspension volumes of 5 and 1 mL/L culture respectively. Solid sodium chloride was added to all hot cycles.

8. After all rounds of ITC were complete the protein solution was filtered through a 0.22  $\mu\text{m}$  syringe filter and stored at 4°C or lyophilized until needed.

### Inverse Transition Cycling Protocol for Construct ( $V_3(VH)_3$ )<sub>4</sub>

Since the protein construct ( $V_3(VH)_3$ )<sub>4</sub> has the ability to accept a charge, the protein purification procedures included a solution pH change to increase or decrease the solutions transition temperature.

1. The purification procedure began with the cell lysate solution after sonication. At this stage, the pH of the protein solution was adjusted between 3 and 4 using 1 M HCl. During the addition of acid additional impurities were precipitated from solution while the protein construct remained in solution.
2. Next, the acidic protein solution was cooled in an ice-bath below 5°C and cold centrifuged (3°C, 20,000xg, 20 min) to remove insoluble cellular material.
3. After cold centrifugation the acidic aqueous protein solution was decanted from the insoluble material then the pH of the supernatant adjusted between 7 and 8 using 1 M NaOH. Also, solid sodium chloride was added to provide a final solution concentration of 2 M NaCl.
4. This solution was quickly heated to 55°C using a 70°C hot water bath.
5. Once heated to temperature the protein solution was allowed to sit in an incubator for 30 minutes at 55°C. During this time the ELP and additional impurities separated from solution.

6. After this incubation period, the aggregated ELP and supernatant phases were separated by hot centrifugation (40°C, 20,000xg, 10 min) followed by decanting of the supernatant phase.  
  
Note: Due to the addition of acid additional impurities were removed in the first stage of purification. This left a smaller pellet size at this stage compared to that obtained from purifications of other constructs without the addition of acid. Also, the appearance of the pellet looks more viscous or “coacervate-like” and does not contain the addition of particulate matter commonly observed in other purifications at this stage. It may be beneficial to investigate this purification method on other ELP constructs.
7. Because of the coacervate appearance and size the re-suspension volume was reduced to 5 mL/L culture deionized water.
8. Once re-suspended, the protein solution was centrifuged cold (3°C, 20,000xg, 10 min) to remove insoluble impurities.
9. After centrifugation the soluble fraction was decanted.
10. This solution was quickly heated to 55°C using a 70°C hot water bath.
11. Once heated to temperature the protein solution was allowed to sit in an incubator for 30 minutes at 55°C. During this time the ELP and any remaining impurities separated from solution.
12. After this incubation period, the aggregated ELP and supernatant phases were separated by hot centrifugation (40°C, 20,000xg, 10 min) followed by decanting of the supernatant phase.

13. The aggregated ELP was re-suspended in 1 mL/L culture, cooled in an ice-bath and filtered through a 0.22  $\mu\text{m}$  syringe filter.

14. After filtration the solution was stored at 4°C or lyophilized until needed.

## Appendix C

Solute linearity check at 280 nm wavelength.

